Quaternary Science Reviews 295 (2022) 107771

Contents lists available at ScienceDirect

Quaternary Science Reviews

journal homepage: www.elsevier.com/locate/quascirev

Hydroclimate reconstruction through MIS 3 in the Middle Paleolithic site of Crvena Stijena (Montenegro) based on hydrogen-isotopic composition of sedimentary *n*-alkanes

Margarita Jambrina-Enríquez [a, b, *], Carolina Mallol [b, c, d], Gilbert Tostevin [e], Gilliane Monnier [e], Goran Pajović [f], Nikola Borovinić [g], Mile Baković [g]

[a] *Departamento de Biología Animal, Edafología y Geología, Facultad de Ciencias, Universidad de La Laguna, 38200, Canary Islands, Spain*
[b] *Instituto Universitario de Bio-Organica Antonio González (IUBO), Universidad de La Laguna, 38206, Canary Islands, Spain*
[c] *Departmento de Geografia e Historia, Universidad de La Laguna, 38200, Canary Islands, Spain*
[d] *Interdisciplinary Center for Archaeology and the Evolution of Human Behaviour (ICArEHB), Universidade do Algarve, Campus de Gambelas, Edificio 1, 8005-139, Faro, Portugal*
[e] *Department of Anthropology, University of Minnesota, Minneapolis, MN 55455, USA*
[f] *National Museum of Montenegro, 81250, Cetinje, N. Cerovića bb., Montenegro*
[g] *Center of Conservation and Archaeology, Cetinje, Montenegro*

A R T I C L E   I N F O

Article history:
Received 26 March 2022
Received in revised form
13 August 2022
Accepted 13 September 2022
Available online 2 October 2022

Handling Editor: Dr. Mira Matthews

Keywords:
Leaf waxes
Hydrogen isotopes
Paleohydrology
Balkan Peninsula
Last glacial-interglacial transition
Middle Paleolithic
Black layers

A B S T R A C T

This study presents a hydroclimatic reconstruction from Crvena Stijena (Montenegro, Balkan Peninsula), a rock shelter that has yielded evidence for Middle Paleolithic human occupation. The integration of lipid biomarkers, hydrogen (δD) isotopic compositions of *n*-alkanes, and organic elemental geochemistry in the 7-m deep vertical sedimentary sequence enables reconstruction of the main hydrological and environmental changes during the MIS 3 and their correlation with the presence at the site. We apply agglomerative hierarchical clustering and principal component analysis to the geochemical, molecular, and stable isotopic data to obtain a robust hydrological record. We find evidence of three aridity trends from the studied period, one of them correlated with the Heinrich Event 5, and humid and cold-temperate conditions in archaeology-rich layers. Our dataset also contributes to the knowledge of past hydrological variability in the Balkan Peninsula, a sensitive area to short-lived climatic shifts, and overall, in the Mediterranean region during the last glacial/interglacial cycle.

1. Introduction

Temperature, aridity and humidity changes, the occurrence of abrupt millennial-scale oscillations and overall climatic variability may have been influential in the distribution and movement of past human populations (Gilligan, 2007; Cohen and Gibbard, 2019). Since the Neanderthals appeared in Europe around 430 Ka (Meyer et al., 2014, 2016) during Marine Isotope Stage 12 (MIS 12; ~478–424 Ka) and for a long expanse of time covering MIS 3 up to ~40 Ka (Benazzi et al., 2011; Higham et al., 2014), human populations experienced glacial/interglacial cycles and numerous abrupt climatic fluctuations. Looking at the site frequency as a rough proxy of Neanderthal presence, there are more sites around globally warm MIS 5e and MIS 3 than around cold MIS 4 (van Andel and Davies, 2003; Mallol et al., 2019). The apparent reduction in the number of Neanderthal sites from the end of MIS 5 through MIS 4 could be related with the long-term global cooling trend associated with MIS 5a-4. MIS 5e (~125-119 Ka) was one of the warmest interglacial periods of the last 800 Ka (Jouzel et al., 2007; Lang and Wolff, 2011) and MIS 3 (~60-27 Ka) was a highly unstable climatic period with six cold periods (Heinrich events, HE) and fourteen warm periods (Dansgaard–Oeschger events, D-O) (Heinrich, 1988; Dansgaard et al., 1993; Rasmussen et al., 2014).

In Europe, the terrestrial response to HE and D-O oscillations

* Corresponding author. Departamento de Biología Animal, Edafología y Geología, Facultad de Ciencias, Universidad de La Laguna, 38200, Canary Islands, Spain.
E-mail address: mjambrin@ull.edu.es (M. Jambrina-Enríquez).

https://doi.org/10.1016/j.quascirev.2022.107771
0277-3791/

have been recorded as rapid changes in precipitation and temperature as evidenced in lacustrine sedimentary sequences (Lago Grande di Monticchio, Ohrid and Prespa; Lézine et al., 2010; Vogel et al., 2010; Panagiotopoulos et al., 2014; Sinopoli et al., 2018) and speleothems (Weber et al., 2018; Columbu et al., 2020). These climatic events have also been identified through multiproxy studies at different Middle Palaeolithic human occupation sites (e.g., Courty and Vallverdu, 2001; d'Errico and Goñi, 2003; Boschian et al., 2017; Biltekin et al., 2019), covering short or discontinuous periods of time.

Here we focus on the Middle Palaeolithic site of Crvena Stijena (CS) (Montenegro, Balkan Peninsula) to provide a picture of climatic and environmental changes at the last interglacial/glacial cycle (MIS 5-2) and to understanding the relationship between past climate changes and human adaptation. Excavations of the CS rock shelter in the mid 1950's through the early 1960's uncovered a 20-m deep sedimentary sequence spanning from the Middle Paleolithic through the Bronze Age (Basler, 1975); later from 2004 to 2015, Mesolithic and late Middle Paleolithic deposits were excavated (Baković et al., 2009; Whallon, 2017) and from 2016 to the present excavations have continued within the Middle Paleolithic deposits (Monnier et al., 2020).

CS is a karstic rock shelter with a 20-m deep sedimentary sequence that comprises thirty-one lithostratigraphic units (Brunnacker, 1975) covering from MIS 4 (Unit XXIV, at 9.5 m depth, a 52.2 ± 6.6 Ka-TL date) to the early Holocene (Unit II, 8.4 ka cal BP-an AMS date at 50 cm depth) (Morley, 2017) and anchored by a tephra layer date (Unit XI, at 7.5 m depth, a Y5 tephra date from the Campanian Ignimbrite at 39.9 ka, Morley and Woodward, 2011). However, the chronology of the lower part of the sequence (Unit XXIV) is uncertain, considering the oldest thermoluminescence (TL) date (70.0 ± 6.2 ka) and electron spin resonance (ESR) date (78.3 ± 0.3 ka) data, which extend the sequence to MIS 5a (Mercier et al., 2017). Independently of the uncertainties associated with the chronometric data from different dating methods (Mercier et al., 2017), archaeological assemblages (Mihailović and Whallon, 2017; Mihailović et al., 2017a) combined with sedimentology and bulk chemical analysis (Morley, 2017), zooarchaeological (Morin and Soulier, 2017) and anthracological data (Shaw, 2017) appear to indicate that the upper part of the CS sequence (Units XI-XIII, 7.5–9 m depth) correlates with MIS 3 (see Whallon and Morin, 2017), a key period in human evolution involving the demise of the Neandertals and their replacement by Anatomically Modern Humans. These studies, compiled in Whallon (2017) and previous work by Brunnacker (1975) have provided valuable archaeological and environmental insights, together with results from recent archaeomagnetic (Bradák et al., 2021) and rRNA sequencing (Jones et al., 2021) studies.

Regarding sedimentary organic matter (OM), the archaeology-rich units (combustion-rich layers: Units XXIV, XXII and XX), have been the object of molecular and isotopic analyses mainly focused on tracing the source of animal fats and exploring combustion temperatures. Different proxies have been measured to this end: 1) fatty acid and sterol identification and palmitic and stearic acid carbon isotope composition, i.e. $\delta^{13}C_{16:0}$ and $\delta^{13}C_{18:0}$) from Unit XX and the middle of Unit XXIV (archaeology-rich) and Unit XXIII (natural sedimentation: coarse gravelly layers) (March et al., 2017), 2) *n*-alkyl nitrile identification and isotopic ($\delta^{13}C_{16:0}$ and $\delta^{13}C_{18:0}$) composition in combustion features from the middle of Unit XXIV (Jambrina-Enríquez et al., 2019), 3) identification of *n*-alkanes, aromatics, *n*-ketones and fatty acids and isotopic ratios ($\delta^{13}C_{16:0}$ and $\delta^{13}C_{18:0}$) on resin-impregnated sediment slabs by Rodríguez de Vera et al. (2020) from the middle of Unit XXIV, and 4) micro-Raman spectroscopic measurements on micromorphological thin sections of microscopic char particles from the middle of Unit XXIV (Lambrecht et al., 2021).

Past vegetation studies through molecular approaches (*n*-alkanes and sterols) at the site are limited and focus on combustion structures from Units XX and the middle of Unit XXIV, and on a coarse gravelly layer (natural sedimentation) from Unit XXIII (March et al., 2017). The latter *n*-alkane study pointed to a grass and herb input, except for one sample associated whit the white/ash layer in Unit XX, which yielded presence of deciduous or coniferous trees, although the sample showed signs of degradation (March et al., 2017). Despite these insights on the OM sources and the degree of OM preservation, they pertain only to three units, and the potential of possibly preserved primary *n*-alkanes and their compound-specific stable hydrogen composition to reconstruct past hydroclimatic changes remain unexplored. Thus, here we investigate the origin and preservation of OM in the CS sequence (from Unit X to XXV) by analysing *n*-alkane distributions and explore the use of long-chain length *n*-alkanes δD values as a potential indicator for reconstructing past hydroclimatic conditions.

Leaf wax-derived *n*-alkanes and their compound-specific stable hydrogen ($\delta D_{alkanes}$) are used for paleovegetation and paleohydrological reconstructions in lacustrine records (e.g., Rach et al., 2014; García-Alix et al., 2021) and in archaeological sequences (e.g., Collins et al., 2013; Connolly et al., 2019). Long-chain *n*-alkanes (nC_{27}, nC_{29}, nC_{31}) are produced by higher land plants and stay well-preserved in sediments because of their resistance against bacterial degradation (Eglinton and Hamilton, 1967). $\delta D_{alkanes}$ in long chain *n*-alkanes record the isotopic composition of precipitation (Sachse et al., 2006, 2012; Hou et al., 2018), which is determined by air temperature and moisture source in temperate regions and by the amount effect accounts in tropical and subtropical regions (Dansgaard, 1964; Sachse et al., 2012; Kahmen et al., 2013).

The CS sequence comprises natural (coarse gravels) and anthropogenic (combustion features) units. There are at least five archaeology-rich units dominated by combustion-derived sediment features (XXIV, XXII, XX, XVIII, XII-M2C) intercalated with archaeology poor unit of natural sedimentation. Combustion features are characterized by a sedimentary sequence of thermally altered sediment at the base, overlain by the charred topsoil (black layer) and capped by the ash layer (white layer) (Mallol et al., 2017). Black layers from simple anthropogenic combustion features reach average temperatures ≤300 °C (Mallol et al., 2013; Aldeias et al., 2016; Buonasera et al., 2019). At ≤ 350 °C, incomplete combustion protects OM from oxidation and microbial activity preserving their original molecular fingerprint (Braadbaart and Poole, 2008; Wiesenberg et al., 2009; Knicker et al., 2013; Diefendorf et al., 2015a; Jambrina-Enríquez et al., 2018) and δD *n*-alkane values remain unaltered preserving their near-primary isotopic signature (Wang et al., 2017; Connolly et al., 2021). In fact, the presence of long-chained nitriles in black layers from the middle of Unit XXIV implies combustion at temperatures around 300–350 °C (Jambrina-Enríquez et al., 2019). These insights provide the opportunity to obtain a complete hydroclimate reconstruction from the CS Middle Paleolithic sequence based on hydrogen-isotopic composition of sedimentary *n*-alkanes.

Rock shelters function as a sediment trap encompassing natural deposition because of regional environment changes, as well as anthropogenic sediment since they have been used as natural shelters by humans (Mentzer, 2017; Goldberg et al., 2009; Miller et al., 2013). Post-depositional processes may affect these deposits resulting in gaps in the sedimentary sequence (Kuehn and Dickson, 1999). The CS sequence is mostly continuous except for a hiatus recorded between Units X and XI by the Y5 tephra layer (Morley, 2017). The sedimentary CS sequence may be key to understanding past climate changes in the Balkan peninsula and overall Mediterranean region and to place the human occupations in the context of past environmental changes. The Central Balkans are a key region for paleoclimate reconstructions because they are a transitional area between two bioclimatic regions (with a temperate-continental climate in the north and a Mediterranean climate in the south) (Rivas-Martínez, 1987) and are also key for the study of hominid migration due to the likely corridor route of the western Europe (Kozłowski, 2004).

In this paper we report the results of molecular (*n*-alkanes), isotopic (compound-specific stable hydrogen isotope compositions of long-chain *n*-alkanes) and organic geochemical analyses (total organic carbon and total sulfur) performed on the vertical sedimentary sequence of the Middle Paleolithic rock shelter of Crvena Stijena (Montenegro). We investigate past hydroclimatic changes in the CS sequence to i) identify climatic fluctuations at time that correlate these with human occupation episodes ii) contribute to interpretations of the CS sequence chronology and its correlation with MIS stages reported by geological and faunal models (Whallon and Morin, 2017) and iii) contribute to existing paleoclimate reconstructions for the Balkan peninsula and overall, for the Mediterranean region during the last glacial/interglacial cycle.

2. Site description

Crvena Stijena (CS) (42°46′40.4″N, 18°28′53.9″E, 700 m a.s.l., southwest Montenegro) is located between Nikšić and the border of Bosnia and Herzegovina, in the eastern side of the artificial Lake Bileća (Fig. 1a and b). This south facing cave is formed in a steep cliff with a large talus slope which runs down to Lake Bileća and is approximately 26 m wide by 15 m high, with a horizontal depth of around 25 m (Morley, 2017) (Fig. 1c). The karstic rock shelter was formed via dissolution of Mesozoic dolomite within the limestone bedrock and tectonic shattering (large sub-vertical faults in the cliff) (Brunnacker, 1975; Morley, 2017). The climate is transitional Mediterranean and humid temperature type, characterized by hot and dry summers (Temperature <22 °C) and temperate and rainy winters (Temperature ranging from −3 to 18 °C). The CS area show an average annual precipitation of ca. 2000 mm and an average annual air temperature of 10.7 °C (climate period 1961/90, Nikšić meteorological station located 45 km from CS) (Burić et al., 2014a) (Fig. 1d). The Mediterranean Oscillation index (MO) strongly influences the climate in this region, there is a strong correlation with rainfall parameters for winter season during negative MO mode (Burić et al., 2014b).

Present-day vegetation around CS is characterized by sub-Mediterranean and Mediterranean climatogenic communities up to 700 m a.s.l. (forest of pubescent oak-*Quercus pubescens* and eastern hornbeam-*Carpinus orientalis*), and epi-Mediterranean and Mediterranean-montaine climatogenic communities over to 950 m asl (forests of pubescent oak and European hophornbeam-Ostrya carpinifolia). At the highest altitude (1893 m asl) appear forest of Heldrich's pine (*Pinetum heldreichii* s.lat.), a Tertiary relic of the Balkan peninsula (Jovanović et al., 1986; Ćulafić et al., 2017).

Modern precipitation δD values were obtained from the Online Isotopes in Precipitation Calculator (OIPC, Bowen and Revenaugh, 2003). Modeled-OIPC mean annual precipitation δD (δDMAP) is −47‰ (95% CI). Higher precipitation δD values were recorded

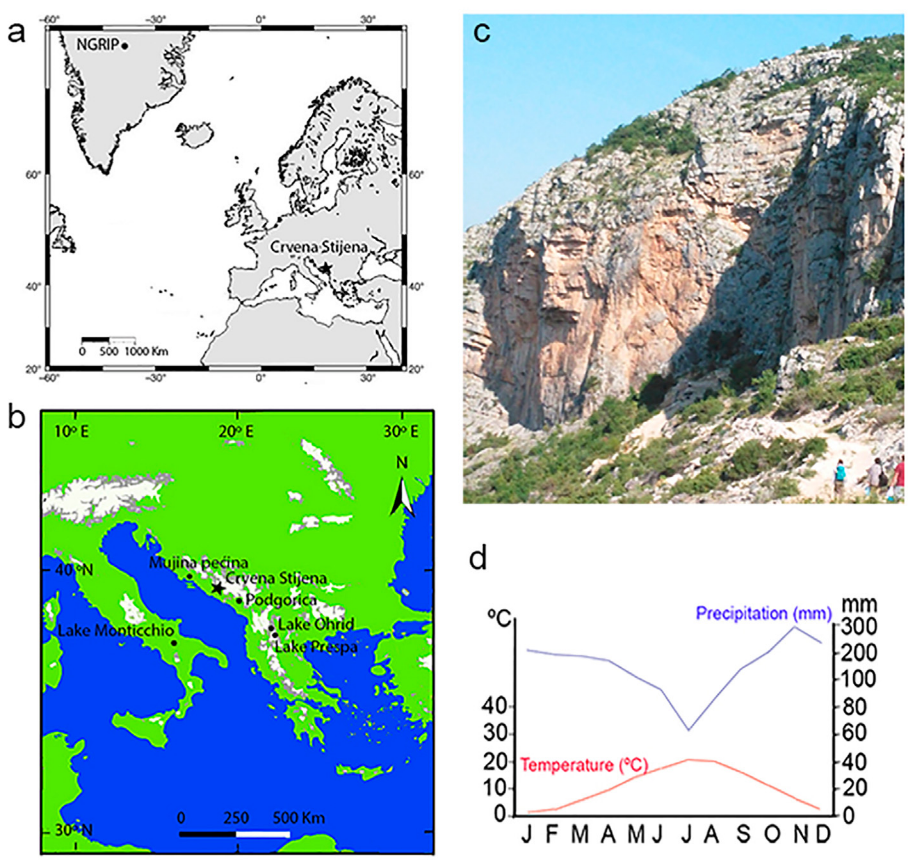

Fig. 1. Location of Crvena Stijena (CS) along with other records mentioned in the text: a) NGRIP ice core (North Greenland Ice Core Project Members, 2004), b) Lake Monticchio Lake Ohrid (Lézine et al., 2010; Vogel et al., 2010; Sinopoli et al., 2018); Lake Prespa (Panagiotopoulos et al., 2014), Middle Paleolithic site of Mujina Pećina (Boschian et al., 2017). c) View of the CS karstic rockshelter; d) Mean monthly air temperature and precipitation for Nikšić meteorological station (Burić et al., 2014a).

from May to September (δD ranges from −35‰ to −23‰) and lower precipitation δD values from October to April (δD ranges from −62‰ to −44‰). The OIPC model estimated that mean autumn-winter precipitation δD values were ca. 23‰ D-depleted relative to those obtained in spring and summer. Similarly, δD values in modern precipitation at Montenegro (Podgorica), from an annual cycle (March 2017–February 2018), recorded more negative values δD in winter (mean value δD = −34‰) and less negative values in summer (mean value δD = −28‰), with a mean annual precipitation δD of −31‰ (Živković et al., 2020). However, the OIPC underestimates δD on the annual scale (a mean annual value of −47‰ *vs*. measured −31‰).

3. The sedimentary sequence

Crvena Stijena has one of the longest Middle Palaeolithic sequences covering from the end of MIS 5a (~78 ka, Unit XXIV) to the early Holocene (8.5 ka, Unit II) (Mercier et al., 2017). Previous sedimentological analysis (particle size, mineralogical and chemical analyses) carried out by Brunnacker (1975) on 20 m long sequence defined thirty-one lithostratigraphic units (SU) (I, top– XXXI, base). Later, Morley (2017) characterized the Units X-XXIV (9.5 m long sequence) based on particle size, magnetic properties, charcoal counts, and bulk chemical analyses and defined three main lithofacies based on different modes of deposition (Morley, 2017). Sedimentological description and radiometric dating are detailed in Morley (2017) and Mercier et al. (2017), but in summary, the sedimentary sequence from the top (Unit X) to the base (Unit XXIV) is comprised by:

(i) Lithofacies 1: a ~3 m thick of well bedded and coarse orange limestone gravels in a sandy matrix. It comprises the Units X (13.4–28.0 Ka, ~1.10 m thick, higher carbonate and low OM values, low magnetic susceptibility (MS) and absence of charcoal and bone fragments), XI (39.0 Ka, ~10 cm thick of ashes identified as the Y-5 tephra-Campanian Ignimbrite (Morley and Woodward, 2011), XII (37.6–43.2 Ka, ~1.25 m thick, high carbonate and low OM content) and XIII (44.2 Ka, ~65 cm thick, high carbonate and low OM contents and high MS values, very occasional charcoal, and no faunal fragments).

(ii) Lithofacies 2: a ~6 m thick of yellowish brown to brownish black coarse gravels and fine-grained layers with abundant anthropogenic material (ash, charcoal, bone fragments and burnt flint). It comprises the Units XIV (~20 cm thick, low carbonate and low MS values, high OM content, variable amounts of charcoal and absence of faunal fragments), XV (~15 cm thick, variable carbonate content and very low OM and MS values, the charcoal content and faunal fragments are low, but the base is rich in charcoal), XVI (~5 cm thick, variable carbonate and OM values, high MS values, low charcoal content, burnt limestone clast), XVII (~1 m thick, high carbonate and low OM content, variable MS and abundant charcoal and faunal -often burnt- fragments), XVIII (~30 cm thick, low carbonate content, high OM and MS values, frequent charcoal fragments), XIX (~25 cm thick, high carbonate and low OM values, low charcoal content and absence of faunal material), XX (48.3–65.5 Ka, ~25 cm thick, charcoal and ash-rich layer, variable carbonate and OM values), XXI (~25 cm thick, low carbonate values and variable charcoal and bone remains), XXII (~30 cm thick, low carbonate and MS values and high OM content, frequent charcoal and burnt bones remains), XXIII (~25 cm thick, high carbonate and low OM content, low charcoal and bone fragments) and XXIV (52.2–78.3 Ka, ~2 m thick, low carbonate values in the base but high at the top, high OM content, extremely rich in charcoal, ash, burnt and unburnt bone fragments, and reddened materials limestone clasts).

(iii) Lithofacies 3: a 75 cm of yellow-orange coarse gravels in a sandy matrix without anthropogenic material. It comprises the Unit XXV (~20 cm thick, high carbonate values, high MS values, low charcoal content and no faunal remains).

4. Sampling and methods

4.1. Samples

The CS sequence presented in this study is composed of three profiles (Fig. 2). In field (June 2017), SUs from Brunnacker (1975) and Morley (2017) were identified, and three stratigraphy columns were designed based on field-macroscopic observations (Fig. 2). Profiles were cleaned before being subsampled removing the surface (~3 cm deep) to remove surface microbial biomass. 76 samples were collected using sterilized tools, wrapped in Al-foil, and preserved at 4 °C before laboratory analysis. From the ~2 m thick of SU XXIV we only had accessibility to the first 40 cm (top of the SU) and the last 50 cm (base of the SU). From the top to the base, the 7 m-deep sedimentary sequence is comprised by:

i) Profile 1. 68 cm vertical long profile located close to the SW wall. This profile comprises from the top to the base the SUs: X (7-cm-thick, 1 sample), XI (12-cm-thick, 1 sample) and XII (M1: 30-cm-thick, 1 sample; M2: 8-cm-thick, 1 sample and M2C: 10-cm-thick, 1 sample.

ii) Profile 2. 462 cm vertical long profile located in the innermost part of the shelter (NE side). This profile comprises from the top to the base the SUs: XII (33-cm-thick, 3 samples every 10 cm), XIII (70-cm-thick, 3 samples every 15 cm), XIV (8-cm-thick, 1 sample), XV (30-cm-thick, 1 sample at the base of the SU, no samples were collected from the clast-supported coarse gravels), XVI (10-cm-thick, 1 sample), XVII (60-cm-thick, 4 samples every ~10 cm, no samples were collected from the clast-supported coarse gravels), XVIII (25-cm-thick, 5 samples every ~5 cm), XIX (30-cm-thick, 5 samples every ~5 cm), XX (40-cm-thick, 11 samples every ~5 cm, including 3 samples from each of the 3 white layers and 3 samples from each of the 3 black layers), XXI (20-cm-thick, 2 samples every 10 cm), XXII (63-cm-thick, 10 samples every ~5 cm, including 2 samples from each of the 2 white layers and 1 sample from each of the 1 black layer), XXIII (30-cm-thick, 2 samples every 15 cm) and XXIV (43-cm-thick, 4 samples every ~10 cm).

iii) Profile 3. 160 cm vertical long profile located in the innermost part of the shelter (NW side). This profile comprises from the top to the base the SUs: XXIV (50-cm-thick, 15 samples including 4 samples from each of the 4 white layers, 6 samples from each of the 6 black layers, 2 samples from each of the 2 red layers and 3 natural sediments at the top and base of the unit), XXV (100 cm-thick, 3 samples every ~30 cm) and XXVI (20 cm-thick, 1 sample).

4.2. Elemental organic analysis

Total carbon (TC), total organic carbon (TOC), total inorganic carbon (TIC) and total sulfur (TS) analyses were performed with a LECO SC 144DR elemental analyser (LECO Corporation, St Joseph, MI, USA) at the Instituto Pirenaico de Ecología (IPE-CSIC), Spain. For TOC analyses, carbonates were removed by acidification with HCl

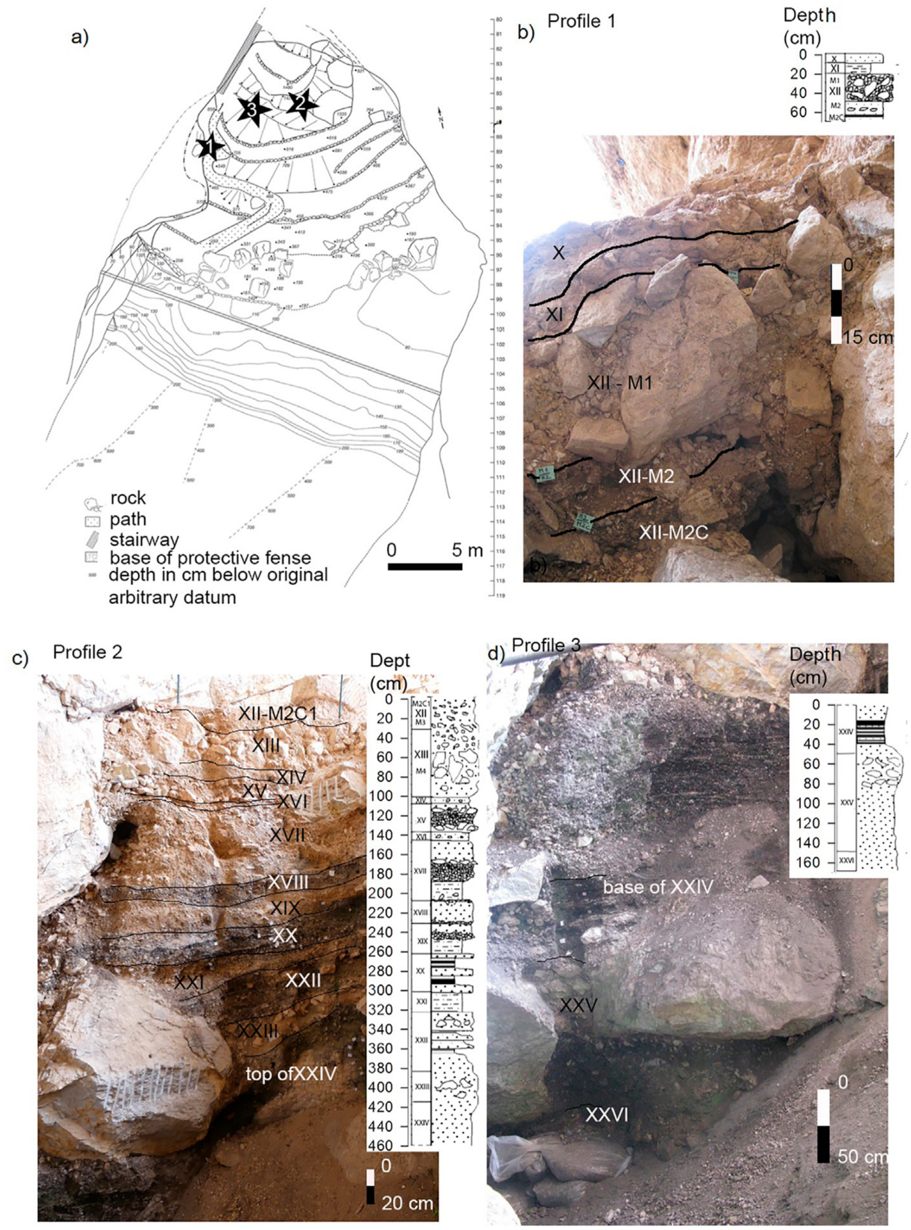

Fig. 2. a) Plan of CS (modified from Whallon, 2017). Stars mark the locations for sedimentary profiles; b, c, and d) view of the profiles and the sedimentary sequence.

1:1. Precision of the TOC and TS measurement were 1% RSD or ±25 ppm (RMS 0.053648) and 1% RSD or ± 2.5 ppm (RMS 0.044829) respectively. TOC/TS ratio was used to track changes in redox conditions.

4.3. n-Alkane extraction, identification and quantification

The *n*-alkanes from 1 to 5 g of each oven-dried (60 °C during 24 h) and homogenized sample were extracted using *QuEChERs* method with some modifications (Herrera-Herrera et al., 2020) which combine a solid-liquid extraction and a dispersive solid-phase extraction. 10 mL of dichloromethane (DCM) as extraction solvent was added to each sediment in a polytetrafluoroethylene (PTFE) tube with a spherical glass ball, and the tube was shaken for 1 min. After addition of 1 μL of 5α-androstane (2000 mg/L in DCM, purity ≥99.9%, Sigma-Aldrich) as internal standard (IS) and 30 s of shaking, 4 g of $MgSO_4$ and 1 g of NaCl were added into the PTFE tube and shaken during 1 min before centrifugation (4700 r.p.m. for 5 min). The supernatant was transferred to another PTFE tube containing 150 mg of $MgSO_4$ and 25 mg of primary secondary amine as clean-up sorbent, shaken for 30 s and centrifuged at 4700 r.p.m. for 5 min. The supernatant which contains the *n*-alkanes was transferred to GC-MS vials and evaporated under nitrogen flow using an Organomation evaporator. Before the injection into the GC–MS system the residue was redissolved in 50 μL of hexane.

The *n*-alkanes analysis was performed using a gas chromatography system with a single quadrupole mass spectrometer (GC-Agilent 7890B, MSD Agilent 5977A) equipped with a HP-5MS capillary column ((5%-phenyl)-methylpolysiloxane, 30 m × 0.25 mm, 0.25 μm film thickness) and an electron impact interface. The GC was programmed to an initial temperature of 70 °C for 2 min, heated with a rate of 12 °C/min to 140 °C and to final temperature of 320 °C for 15 min with a heating rate of 3 °C/

min and a total run time of 82.83 min, using a Helium carrier gas (2 mL/min). The multimode injector was held at a split ratio of 5:1 at an initial temperature of 70 °C during 0.85 min and heated to 300 °C at a rate of 720 °C/min. The MS was operated in full scan mode (*m/z* 40–580) with an electron ionization energy of 70 eV and with the temperatures of the ion source and quadrupole set at 230 °C and 150 °C, respectively. All measurements were repeated three times.

n-Alkanes and IS were identified taking the four most intense fragment ions (m/z 43, 57, 71 and 85 for *n*-alkanes, and m/z 67, 95, 81 and 245 for IS) and by comparison of their retention times and mass spectra with those of reference compounds (C_8–C_{40} mix and 5-α-androstane, Supelco). *n*-Alkanes were quantified using calibration curves obtained by plotting the area/areaIS ratio versus the concentration of each reference compound. Correlation coefficients were >0.995. The *n*-alkane concentrations were normalized to sample weight (dry sediment) and expressed as μg of individual compound per gram of dry sediment (μg/gds). All the *n*-alkanes analysis (extraction, identification, and quantification) were performed at the Archaeological Micromorphology and Biomarker Laboratory (AMBI-Lab), Universidad de La Laguna, Tenerife (Spain).

4.4. Compound-specific stable hydrogen isotope analysis in n-alkanes

Hydrogen isotopic composition of long sedimentary *n*-alkanes (nC_{29} and nC_{31}) was measured with a Thermo Scientific Isotope Ratio Mass Spectrometer Delta V Advantaged coupled to a GC Trace1310 through a Conflo IV interfaced with a temperature converter GC Isolink II equipped with a silica capillary column ((5%-diphenyl)-dimethylpolysiloxane, 30 m × 0.25 mm, 0.25 μm film thickness) and a Trace Gold 5-MS (Thermo Fisher Scientific, Bremen, Germany). Pyrolysis was performed in a microvolume ceramic tube at 1420 °C. The Programmed Temperature Vaporising injector (PTV) was held in splitless mode (splitless to split 1:50). The temperature started from 60 to 79 °C (held 30 s with a rate of 10 °C/min), then increased to 325 °C at 10 °C/s (held for 3 min) and finally was increased to 350 °C and held 3 min (rate 14 °C/s). For the GC oven, a 2 min isothermal period at 70 °C increasing to 140 °C (held 2 min) at a rate of 12 °C/min followed by an increase to 320 °C and held for 15 min at a rate of 3 °C/min. Helium was used as the carrier gas at a flow rate of 1.5 mL/min. Data acquisition and processing were carried out using the Isodat 3.0 software (Thermo Fisher Scientific, Bremen, Germany). To ensure stable ion-source conditions during measurement, the $H3^+$ factor was constant over the 7 weeks measurement period at 3.2 (SD = 0.3). Each sample was analysed in triplicate. Only compounds with sufficient signal intensity (>1500 mV) on the IRMS were used for hydrogen isotopic data evaluation. The δD measurements were normalized to the Vienna Standard Mean Ocean Water (VSMOW) and calibrated with a standard containing nC_{16} to nC_{30} alkanes (MIX A6 obtained from Arndt Schimmelmann, Indiana University) of known isotopic composition. The hydrogen isotope values are reported in conventional delta notation (δD values) in per mil (‰) units. In triplicate analyses of samples, standard deviations for *n*-alkane δD were usually better than 5‰.

5. Results

Results are provided in Supplementary Table S1. Gaps between SUs are due to absence of fine-grained sedimentary matrix in clast-supported layers.

5.1. TOC, TIC and TS content

TOC, TIC and TS values vary between 0.04% and 13.84%, 1.05% and 10.90% and 0.01% and 0.86%, respectively. TOC/TS weight ratio varied between 0.01 and 0.50. Higher TOC (>5%) and lower TIC (<5%) values were recorded in Units XX, XXII and XXIV, and lower TOC (<1%) and higher TIC (>8%) values in Units X-XIII, XIX, XXI and XXIII. Higher TS (>0.2%) values were recorded in Units XX, XXII and XXIV. TOC/TS weight ratios were constant along the sedimentary sequence (<0.2) with some peaks in Units XII and XXIV (>0.4).

5.2. n-Alkane concentration and distribution patterns

n-Alkane concentrations (nC_{22} to nC_{35}) ranged from 0.1 to 1.7 μg/gds. Higher concentrations (>0.5 μg/gds) were recorded in Unit XII and in combustion/black layers from Units XX and XXIV, and lower (<0.2 μg/gds) in Unit X and ash layers from Units XX, XXII and XXIV. The *n*-alkane distribution pattern exhibits a mostly unimodal distribution (peaking at nC_{29} or nC_{31}) with a strong odd over even carbon number preference. Some samples from Unit XXII showed a clear even over odd carbon number predominance centered at nC_{28}. nC_{31} was the most abundant *n*-alkane in all the sequence except in Units XII-XV, XXI-XXIII which recorded nC_{29} as the dominant alkane.

The distribution of *n*-alkanes was evaluated using long chain *n*-alkane ratios i.e. $nC_{31}/(nC_{29} + nC_{31})$ and $nC_{31}/(nC_{27} + nC_{31})$ and $(nC_{31} + nC_{33})/(nC_{27} + nC_{29} + nC_{31} + nC_{33})$, the Carbon Preference Index (CPI, Bray and Evans, 1961), Odd over Even Predominance (OEP, Hoefs et al., 2002), and the Average Carbon Length (ACL, Poynter et al., 1989).

$CPI_{25\text{-}33} = [\sum (nC_{25}\ nC_{33})\ odd/\sum (nC_{24}\ nC_{32})\ even + \sum (nC_{25}\ nC_{33})\ odd/(nC_{26}\ nC_{34})\ even]/2$

$OEP_{27\text{-}33} = (nC_{27} + nC_{29} + nC_{31} + nC_{33})/(nC_{26} + nC_{28} + nC_{30} + nC_{32})$

$ACL_{25\text{-}33} = (Ci^*[Ci])/\sum[Ci]$; Ci is the concentration of each *n*-alkane with i carbon atoms, 25< i < 33

All the indices showed a covariant variation along the sedimentary sequence. The CPI and OEP values varied between 1.1 and 7.3, and 0.9 and 7.4, respectively. The ACL values ranged from 28.3 to 30.5. Higher CPI (>5), OEP (>5) and ACL (~30) values were recorded in Units XII (M2), XVIII and XIX, and low CPI (~1), OEP (~1) and ACL (~28) values in samples from Unit XXII with an even-numbered *n*-alkanes predominance.

5.3. Compound specific stable hydrogen isotope ratios in long chain n-alkanes

nC_{29} and nC_{31} alkanes were not abundant enough in all samples to obtain robust δD values (Table S1). The δD values of the odd numbered long chain *n*-alkanes (nC_{29} and nC_{31}) of CS sequence range from −403 ± 3‰ to −141 ± 2‰ and −372 ± 4‰ to −147 ± 3‰ respectively. The long-term δD changes reveal co-variability between nC_{29} (−223 ± 3‰ mean value) and nC_{31} (−232 ± 3‰ mean value) with an increasing trend during the analysed period. The δD values were more negative in the older part of the sequence (Units XXVI/XXV boundary, XXV and XXIV), followed by an increase towards more positive δD values (Units XXIV-X) and occasionally negative values at the top of the sequence (Unit XII-M2C). The average δD values of nC_{29} and nC_{31} changed from −326 ± 4‰ and −321 ± 4‰ (Units XXVI/XXV boundary and XXIV) to −205 ± 3‰ and −210 ± 3‰ (Units XXIV-X) (a difference of 122 and 111‰), respectively.

5.4. Statistical analyses

The analytical data obtained were analysed using SPSS v.26 software. A squared Euclidean cluster analysis was performed with the inorganic and organic proxies and stable isotopic data using Ward's Hierarchical grouping method. This analysis determined three different groups (Fig. 3):

(i) Group 1: Units X, XIII, XVII, base of XXI and XXII, characterized by mean values of 8.2% for TIC, 1.5% for TOC, 0.1 for TS/TOC, 0.3 μg/gds for n-alkane concentration, 29.1 for ACL, 2.2 for CPI, 2.2 for OEP, $\delta D_{C29} = -168‰$ and $\delta D_{C31} = -178‰$.
(ii) Group 2: Units: XII-M2, XIX, XVIII, top of XXI, top of XXIV and XXVI/XXV boundary, characterized by mean values of 8.2% for TIC, 2.1% for TOC, 0.0 for TS/TOC, 0.4 μg/gds for n-alkane concentration, 30.0 for ACL, 5.7 for CPI, 5.7 for OEP, $\delta D_{C29} = -201‰$ and $\delta D_{C31} = -207‰$.
(iii) Group 3: Units: XII-M2C, XX, XXIV and XXV, characterized by mean values of 4.1% for TIC, 6.5% for TOC, 0.0 for TS/TOC, 0.8 μg/gds for n-alkane concentration, 29.9 for ACL, 4.0 for CPI, 4.0 for OEP, $\delta D_{C29} = -294‰$ and $\delta D_{C31} = -291‰$.

A Principal Component Analyses (PCA) was performed after confirming the adequacy of data with the Kaiser–Meyer–Olkin (0.661) and Bartlett's sphericity tests. The rotation method was orthogonal VariMax rotation. The first two components explain 74% of the total variance. The first one accounts for 45.4%, whereas the second one explains 28.3% of the variance. The first component is associated with higher TIC content and D-enriched values at the positive end, and higher TOC content and n-alkane concentrations at the negative end. On the other hand, the second component is related at higher CPI, OEP and ACL indices ant the positive end (Fig. 4). The PCA result in the three main groups is consistent with the three Euclidean groups and is classified from highest to lowest organic content as 3rd Euclidean group, 2nd Euclidean group and 1st Euclidean group (Supplementary Information Fig. S1).

6. Discussion

6.1. Organic matter preservation

The studied CS sequence is comprised of coarse gravels in a sandy matrix with: i) high TIC content, low TOC content, low n-alkane concentrations, and nC_{29} as the dominant n-alkane, identified within the 1st Euclidean cluster group (X, XIII, XVII and XXI-XXII), ii) high TIC content, relatively higher TOC content and n-alkane concentrations and $nC_{29+}nC_{31}$ as dominant n-alkanes, identified within the 2nd Euclidean cluster group (XII-M2, XIX, XVIII, top of XXI, top of XXIV and XXVI/XXV boundary) and iii) low TIC content, high TOC content and n-alkanes concentrations and nC_{31} as the dominant n-alkane, identified within the 3rd Euclidean cluster group XII-M2C, XX, XXIV and XXV (Figs. 3 and 4).

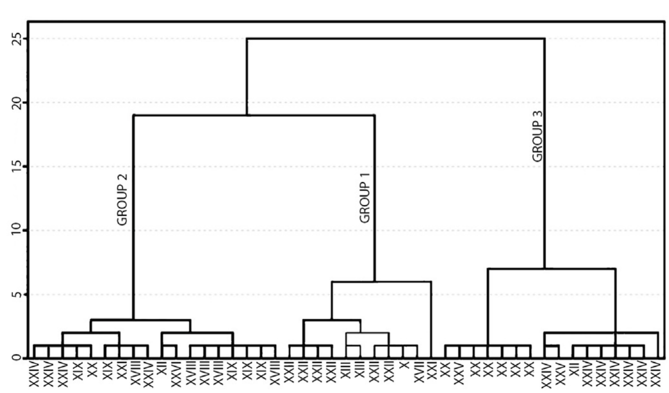

Fig. 3. Clusters for CS samples as a function of inorganic and organic proxies and stable isotopic data (N = 44).

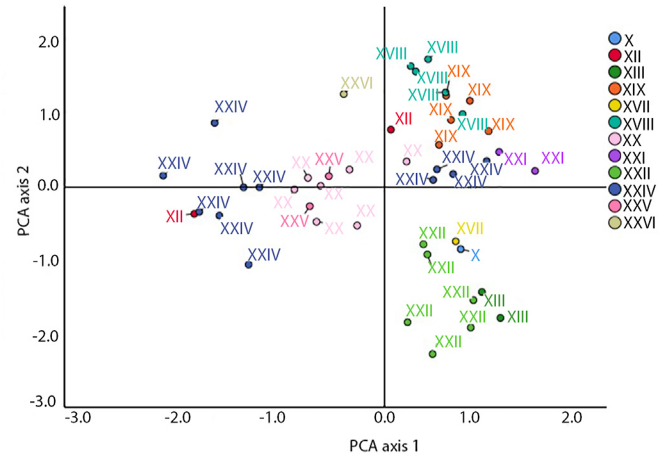

Fig. 4. Plot of the two components obtained by the Principal Component Analysis (PCA).

Potential preservation and the biological source of organic matter can be investigated using the CPI and OEP indices on n-alkanes, which illustrates the differences in the relative concentrations of odd vs. even carbon-number n-alkanes (Bray and Evans, 1961; Eglinton and Hamilton, 1967; Rieley et al., 1991). Terrestrial, submerged/floating, and emergent aquatic plants exhibit CPI and OEP >1, usually higher than 5, while bacteria and algae are at CPI and OEP ~1 (Eglinton and Hamilton, 1967; Cranwell, 1981; Rieley et al., 1991; Li et al., 2020). A CPI~1 also suggests petrogenic input and diagenetic processes, which may produce similar proportions of even and odd carbon alkanes (Bray and Evans, 1961; Hedges and Prahl, 1993). The OM in the CS sequence is well preserved and records higher CPI values (average CPI and OEP values = 3.6, N = 76). However, some bacterial degradation can be attested in SU XXII (natural sediments i.e., coarse gravels) which shows an even-over-odd carbon predominance, with CPI and OEP values ≤ 1 and the lowest ACL values (~28) compared to the other SUs (mean ACL value ~30, N = 72) (Fig. 5). ACL illustrates the average chain length and is used as a paleoclimatic proxy (see section 6.3) rather than to distinguish graminoids from woody plants, since it responds mainly to variation in humidity and temperature (Wang et al., 2015; Bush and McInerney, 2013) and the fact that ACL values are highly variable within plant groups (Bush and McInerney, 2013). On the other hand, degradation with charring temperatures ≥350 °C result in low ACL and CPI values (CPI ~1), therefore, higher CPI and ACL values can be indicative of incomplete biomass burning (≤350 °C) (e.g., Wiesenberg et al., 2009; Knicker et al., 2013; Diefendorf et al., 2015a; Jambrina-Enríquez et al., 2018).

Anthropogenic SUs XXIV, XXII, XX, XVIII and XII comprise natural sedimentation (yellowish-brown to brownish-black coarse gravels) and combustion features. Combustion features are made up of a sedimentary sequence of thermally altered soil or sediment at the base (reddish-brown layer), overlain by the fuel or charred topsoil (dark brown/black layer) and capped by the combustion residues (ash: white/yellowish layer) (Mallol et al., 2017). The dark brown/black sedimentary layer is normally considered as representing the combustion substrate, either carbonized fuel (Leroi-Gourhan, 1973) or the charred ground beneath the fire (Mallol et al., 2013). In Unit XXIV, seven diachronous combustion features

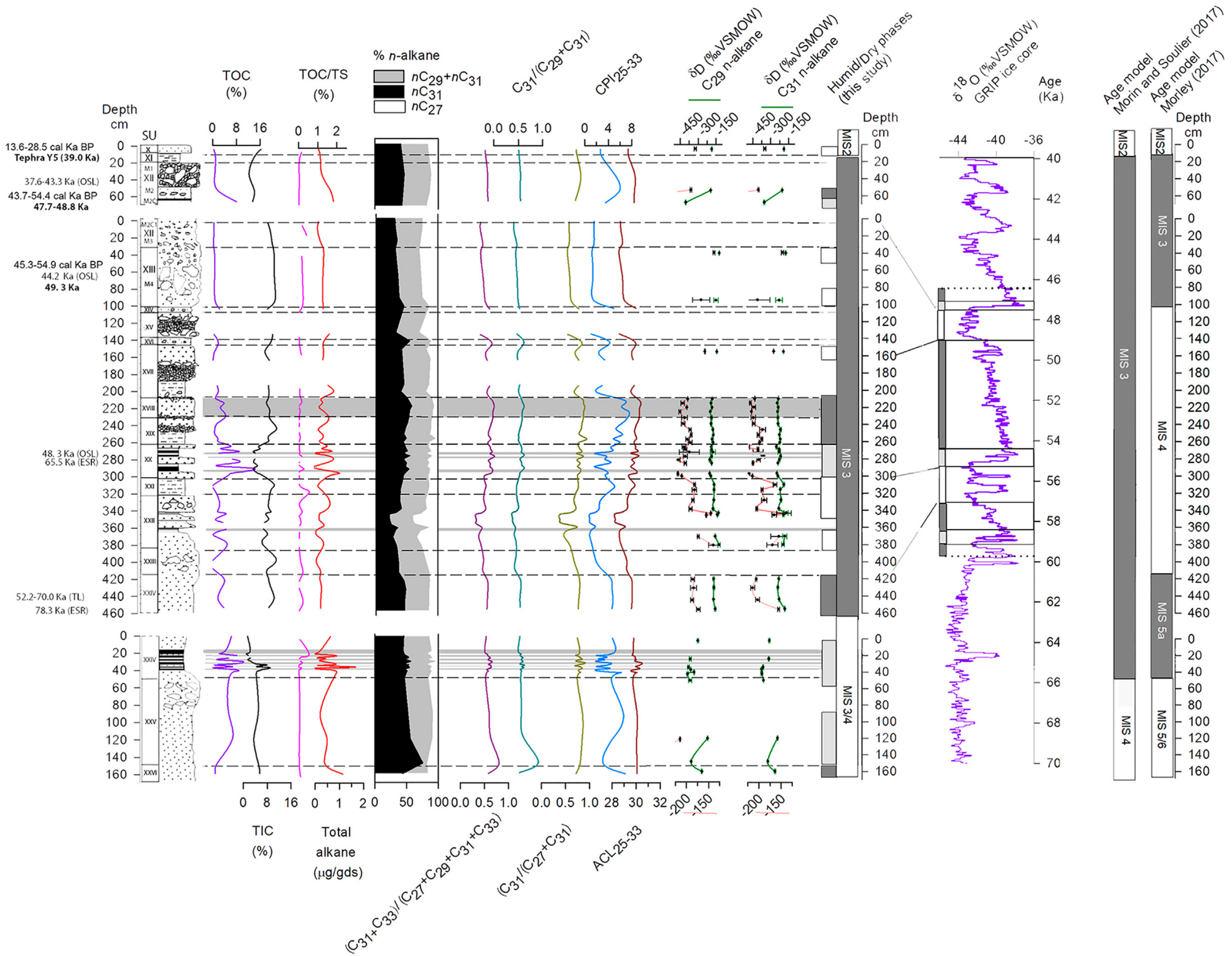

Fig. 5. a) CS stratigraphic column with geochemical and biomarker components (*n*-alkane and δD_{C29}, δD_{C31}) represented with respect to depth (grey bands indicate human occupation layers). Humid and dry phases inferred through our study are indicated with white boxes (cold and dry conditions), dark grey boxes (warm-temperate and humid climate), and light grey boxes (cold-temperate and humid climate). AMS data were recalibrated using the IntCal20 (Reimer et al., 2020); b) comparation with the $\delta^{18}O$ record of the NGRIP ice core (North Greenland Ice Core Project Members, 2007); and c) CS age models based on geological (Morley, 2017) and faunal (Morin and Soulier, 2017) studies (dark grey: warm stages and white: cold stages).

composed by white and/or grey ash facies (white layers) and their underlying black or dark brown facies (black layers) were identified (Morley, 2017; Bradák et al., 2021). Micromorphologial studies in this SU indicated these combustion features are *in-situ* (Morley, 2007). In SU XX, three combustion features intercalated within the natural sedimentary layers were identified, along with one black layer and two white and grey layers intercalated within the natural sedimentary layers in SU XXII, and one black layer in the SU XII (XII-M2C). However, no distinct white and black combustion layers have been reported for SU XVIII. Both anthropogenic (black and white layers) and natural sediments (coarse gravels), reveal a good state of organic matter preservation with clear odd-over-even carbon number alkane predominance and higher CPI and OEP (CPI and OEP between 2 and 6), and ACL values (~30) (Fig. 5). The exception is SU XXII, whose natural sediments show degradation in contrast to the good OM preservation of the black layer.

Thermal degradation of plant biomass under laboratory-controlled conditions has shown that *n*-alkane distributions exhibit a strong odd-over-even carbon chain predominance at low temperatures ($\leq$350 °C for leaves, Wiesenberg et al., 2009; Diefendorf et al., 2015a; Jambrina-Enríquez et al., 2018; and $\leq$250 °C for branches and twigs, Jambrina-Enríquez et al., 2018). Above those temperatures, the CPI and ACL decrease significantly (Wiesenberg et al., 2009; Knicker et al., 2013; Diefendorf et al., 2015a; Jambrina-Enríquez et al., 2018). The good OM preservation of black layers (average CPI and OEP = 4, average ACL = 30, N = 17) suggest that combustion temperatures of black layers are $\leq$350 °C. These findings agree with previous experimental data, which shows that the average temperature associated with black sedimentary layers is $\leq$ 300 °C (Mallol et al., 2013; Aldeias et al., 2016; Buonasera et al., 2019). On the other hand, the good preservation of OM in the CS white layers, which reach combustion temperatures higher than 600 °C (Mallol et al., 2013; Aldeias et al., 2016) (average CPI and OEP = 2, and average ACL = 3, N = 8), could be explained by the presence of charred remains (e.g., charred topsoil residues or microcharcoal) embedded in the ashes as relicts of incomplete combustion.

6.2. Distribution and sources of organic matter

n-Alkanes distribution patterns provide additional insights on the sources of OM (Cranwell et al., 1987; Ficken et al., 2000). An odd-over-even carbon number predominance is produced over long-chains by terrestrial land plants (Cmax: $n\mathrm{C}_{27}$, $n\mathrm{C}_{29}$ or $n\mathrm{C}_{31}$), over mid-chain *n*-alkanes in submerged/floating and emergent aquatic plants (Cmax: $n\mathrm{C}_{21}$, $n\mathrm{C}_{23}$ or $n\mathrm{C}_{25}$) and over short-chain *n*-alkanes in bacteria and alga (Cmax: $n\mathrm{C}_{15}$, $n\mathrm{C}_{17}$, $n\mathrm{C}_{19}$) (Eglinton and Hamilton, 1967; Rieley et al., 1991; Cranwell, 1981; Cranwell et al., 1987; Meyers and Ishiwatari, 1993). The distribution of *n*-alkanes in CS is dominated by long-chain alkanes ($n\mathrm{C}_{25}$-$n\mathrm{C}_{35}$), with high concentrations of $n\mathrm{C}_{29}$ or $n\mathrm{C}_{31}$, both indicative of terrestrial land plant contribution (Bush and McInerney, 2013; Diefendorf et al., 2015b). $n\mathrm{C}_{29}$ is abundant in trees (Schwark et al., 2002; Bush and McInerney, 2013; Diefendorf et al., 2015b), and has been reported as the dominant *n*-alkane during the deposition of SUs XXIII-XXI, XV-XIII, XII_M2C1 and X (1st Euclidean cluster group). On the other hand, $n\mathrm{C}_{31}$ maxima have been documented in grasses (Bush and McInerney, 2013; Diefendorf et al., 2015b) but also in conifers (Schwark et al., 2002; Bush and McInerney, 2013; Diefendorf et al., 2015b) as well as in some angiosperms (Bush and McInerney, 2013; Jambrina-Enríquez et al., 2018), and the dominant *n*-alkane during the deposition of SUs XII-M2, XIX, XVIII, top of XXIV and XXVI/XXV boundary (2nd Euclidean cluster group) and in SUs XII-M2C, XX, XXIV and XXV (3rd Euclidean cluster groups), which include both anthropogenic (black and white layers) and natural sediments (coarse gravels). Some SUs from 1st and 2nd Euclidean cluster groups show bimodal distributions with maximum at $n\mathrm{C}_{29}$ and $n\mathrm{C}_{31}$ (X, XIII, XVII, top of XXI). Theses variations in the dominant *n*-alkanes are also inferred by long-chain *n*-alkane ratios, $(n\mathrm{C}_{31} + n\mathrm{C}_{33})/(n\mathrm{C}_{27} + n\mathrm{C}_{29} + n\mathrm{C}_{31} + n\mathrm{C}_{33})$, $n\mathrm{C}_{31}/(n\mathrm{C}_{29}+n\mathrm{C}_{31})$ and $n\mathrm{C}_{31}/(n\mathrm{C}_{27}+n\mathrm{C}_{31})$ (Fig. 5) and could tentatively represent changes in the environmental drivers of plant communities (e.g., taxa adapted to more humid and less humid conditions).

The CS sequence reveals fluctuations in TIC (carbonate) content, which may reflect different availability of water for: i) carbonate dissolution (low TIC values) and $n\mathrm{C}_{31}$ contribution from taxa adapted to humid conditions (3rd Euclidean cluster group: XII-M2C, XX, XXIV and XXV) or ii) carbonate precipitation processes (high TIC values) and $n\mathrm{C}_{29}$ (1st Euclidean cluster group: X, XIII, XVII and XXI-XXII) and $n\mathrm{C}_{31}$ (2nd Euclidean cluster group: XII-M2, XIX, XVIII, top of XXI, top of XXIV and XXVI/XXV boundary) contributions from taxa adapted to less humid conditions. Although low TIC content mostly pertains to the 3rd Euclidean cluster group, both natural sediments and archaeological layers (combustion features) show low TIC values, suggesting that a climatic humidity signal can be inferred for these units. In fact, SU XXV represents natural sedimentation (archaeologically poor or sterile coarse gravels in a sandy matrix) and shows a low TIC content (3rd Euclidean cluster group, Figs. 3 and 4).

These differences in TIC values and the *n*-alkane dominant are remarkable during the intense human occupation levels (combustion features): $n\mathrm{C}_{31}$ derived from taxa adapted to humid conditions in SUs XXIV, XX and XII-M2C, $n\mathrm{C}_{31}$ derived from taxa adapted to transitional or less humid conditions in SU XVIII and $n\mathrm{C}_{29}$ derived from taxa adapted to less humid conditions in SUs XXII. This is consistent with the archaeomagnetic and magnetic fabric data that suggest water-lain sedimentation processes (SUs. XXIV) (Bradák et al., 2021).

Predominance of long-chain *n*-alkanes in the CS black layers indicates that the fine OM is the charred ground beneath the fire (mainly leaves $n\mathrm{C}_{29}$ o $n\mathrm{C}_{31}$) and not carbonized fuel (branches) which are characterized by higher mid-chain *n*-alkanes concentrations (O'Malley et al., 1997; Knicker et al., 2013; Jambrina-Enríquez et al., 2018); leaves produce higher concentrations of *n*-alkanes (~500 μg per gram of dry sample) than branches (~20 μg per gram of dry sample) (Jambrina-Enríquez et al., 2018). Black layers from a wood-fuelled Middle Palaeolithic combustion structure recorded an odd-over-even *n*-alkane predominance and higher mid-chain alkanes concentrations, suggesting that the branches were topsoil residues and not fuel (Leierer et al., 2019) since the *n*-alkane distribution of charred wood is preserved up to 150 °C (at 250 °C there is a loss of the primary *n*-alkane pattern) (Jambrina-Enríquez et al., 2018). Although the odd-over-even predominance of *n*-alkanes peaking at $n\mathrm{C}_{31}$ in the white layers from SUs XXIV and XX, or $n\mathrm{C}_{29}$ in the SU XXII white layer could be consistent with charred topsoil residues incorporated into the ash from the underlying black layer. However, we cannot rule out microcharcoal contribution, since long-chain *n*-alkanes have been identified in twigs (Jambrina-Enríquez et al., 2018) and given the limited current reference data on charred wood lipid biomarkers (plant species, state of biodegradation, calibre of the wood) (O'Malley et al., 1997; Knicker et al., 2013; Jambrina-Enríquez et al., 2018) and the absence of phytoliths in the ash layer in SU XXIV (Morley, 2007). On the other hand, bone-fuelled fires do not contribute to the concentration of sedimentary alkanes since they are in trace amounts and $n\mathrm{C}_{15}$-$n\mathrm{C}_{17}$ are the dominant alkanes (Buonasera et al., 2019).

The present-day vegetation at CS, the C_3-plant type, has been described by Ćulafić et al. (2017): the sub-Mediterranean and Mediterranean-type climatogenic communities comprise *Petteria* *ramentacea*and *Juniperus oxycedrus* shrubs, *Paliurus pina-christi* and *Ficus carica* at lower elevations, together with *Rhamnus orbiculata, Frangula rupestris, Pistacia terebinthus*, and *Celtis australis*. On the cliffs above CS and growing between rocks, there are *Muscari racemosum, Muscari botryoides, Euphorbia wulfeni, Athionema saxatile, Cerastium glomeratum, Sanguisorba, Seseli globiferum, Sesleria robusta, Tanacetum corymbosum, Ephedra campilopoda.* On the northern and northeastern slopes above CS, appear *Fraxinus ornus, Acer monspessulanum, Carpinus orientalis, Quercus pubescens, Quercus cerris, Corylus avellana, and Petteria ramentacea* (Ćulafić et al., 2017). *n*-Alkane distribution studies of present-day vegetation identified higher concentrations of nC_{31} in *Pinus cembra, Juniperus* and *Abies* (Schwark et al., 2002; Bush and McInerney, 2015 and reference therein), *Celtis australis* (Jambrina-Enríquez et al., 2018), *Carpinus* and *Fraxinus ornus* (Bush and McInerney, 2015 and reference therein) and higher concentrations of nC_{29} in *Pinus sylvestris* and *Quercus* (Bush and McInerney, 2015 and reference therein). Angiosperms produce significantly higher *n*-alkane abundances than gymnosperms (Diefendorf et al., 2011), but Cupressaceae (*Juniperus*) produce significantly higher amounts of *n*-alkanes than pinaceae (*Pinus*) (Diefendorf et al., 2015b).

Based on our observed *n*-alkane distribution pattern and elemental geochemical data, as well as previous micromorphological (Morley, 2007), archaeomagnetic (Bradák et al., 2021) and archaeobotanical (Shaw, 2017) data, we tentatively relate more humid stages (XXV/XXIV and XX) with nC_{31} contribution from taxa adapted to wetter climatic conditions (e.g., *Pinus cembra, Abies*). This is consistent with cold conditions and a predominantly coniferous forested environment, in agreement with archaeozoological and archaeobotanical data from SUs XXIV and XX (Morin and Soulier, 2017; Shaw, 2017). Nevertheless, we cannot rule out an anthropic input to the shelter to explain the presence of grasses and herbs (nC_{31} dominant alkane, e.g., SU XII-M2C). Higher nC_{31} contribution in transitional or less humid stages (XXVI/XXV boundary, top of the XXIV, top of the XXI, XIX-XVIII and XII_M2-XI) with presence of angiosperms (e.g., *Celtis australi*s, *Carpinus, Fraxinus*) and gymnosperms as *Juniperus*, and a higher nC_{29} or $nC_{29+}nC_{31}$ input in less humid stages, i.e., XXIII-XXI, XVII-XIII, XII_M2C1, X with *Pinus sylvestris-Juniperus* derived alkanes and grasses (Fig. 5).

Although present-day forest pines (*Pinetum heldreichii* s.lat) only appear at the highest altitudes (1893 m asl) (Jovanović et al., 1986), anthracological data from CS show the dominance of pine taxa (*Pinus sylvestris*) (Shaw, 2017). In SUs XI-XV and XXII the 89% of the charcoal assemblage is dominated by conifers (*Pinus*: 63%, *Abies* sp., *Juniperus* sp.: 2.5%), and 3% by angiosperms (*Prunus* sp., *Fraxinus* sp., *Fagus* sp., *Cornus* sp., *Juglans* sp, *Salix* sp. and *Sambucus* sp.) (Shaw, 2017). Whereas in SUs XXIV and XX *Pinus sylvestris* and *Pinus peuce/cembra* were the dominant taxa (75%), with less than 2% abundance of other conifer and angiosperm taxa. Although *Pinus sylvestris* was the most abundant taxon in the CS sequence, the 88% of the *Pinus peuce/cembra* fragments at CS were identified in SU XXIV (Shaw, 2017). *Pinus peuce* is a soft pine native to the Balkan Peninsula which requires cool temperatures and high humidity and altitudes above 800 m asl (Alexandrov and Andonovski, 2011). On the other hand, *Pinus sylvestris* grows in the supra-Mediterranean bioclimatic belt and is adapted to cold and humid climates as well as to high altitude areas with sufficient rainfall (above 1000−1200 m asl) (Rivas-Martínez, 1987; Gutiérrez, 1990).

Despite the dominance of pine in the athracological record, we cannot dismiss the fact that charcoal is an anthropogenic element and, although it may inform us about human behaviour and past fuel management, it does not necessarily represent a complete picture of the natural surrounding landscape because it may be reflecting a human selection bias for specific properties conducive of lighting, cooking, smoking, drying, etc. In fact, pollen records from lake sedimentary sequences covering from MIS 5 to MIS 2 in the Balkan peninsula (Lake Ohrid, Albania by Lézine et al., 2010; Lake Prespa, on the Albania/Macedonia/Greece boundary by Panagiotopoulos et al., 2014) show a significative predominance of deciduous taxa such as *Quercus* sp. and *Carpinus* and evergreen conifers (*Juniperus* and *Abies*) during the MIS 3, eventhough no *Quercus* charcoal has been identified so far in the CS sequence (Shaw, 2017). Mediterranean pollen records from lake sequences (e.g., Lake Monticchio, Allen et al., 1999; Lake Ohrid, Lézine et al., 2010; Lake Prespa, Panagiotopoulos et al., 2014) recorded open landscapes with significant temperate-tree presence during the MIS 3, interrupted by cold events (Heinrich events) characterized by *Juniperus* and *Pinus* taxa (Lézine et al., 2010; Panagiotopoulos et al., 2014).

6.3. Drivers of variation in the hydrogen isotope composition (δD) of n-alkanes

Variability of *n*-alkane hydrogen stable isotopic composition is potentially driven by changes in precipitation amount and source, evapotranspiration, atmospheric temperatures and plant types (Gamarra et al., 2016; Sachse et al., 2012; Wirth and Sessions, 2016). We evaluated linear relationships between δD_{C29}, δD_{C31}, *n*-alkane concentrations (nC_{29} and nC_{31}), $ACL_{29+31+33}$ and TIC based on Pearson's regressions by comparing the 95% confidence intervals of intercepts and slopes (Table 1). Moderate correlation of $ACL_{29+31+33}$ and the δD values of C_{29} and the C_{31} record suggests that aridity, which is closely related to evapotranspiration, may have had a moderate influence on hydrogen isotopic composition (Table 1). Temperature and humidity variations can also affect the ACL and CPI values (Dodd and Poveda, 2003; Sachse et al., 2004, 2006; Xie et al., 2004; Rao et al., 2009; Wang et al., 2015; Bush and McInerney, 2015). To reduce cuticular transpiration under warm conditions and aridity, deciduous plants produce longer *n*-alkanes (high ACL values) and under cold and dry climates, evergreen plants also increase the production of longer *n*-alkanes (high ACL values) to protect themselves from winter desiccation and freezing (Dodd and Poveda, 2003; Sachse et al., 2006; Bush and McInerney, 2015). However, increased ACL values have been also related with warm and wet climatic conditions (Sachse et al., 2004; Castañeda et al., 2009; Jambrina-Enríquez et al., 2016). Higher production of odd-over-even *n*-alkanes (high CPI values) have been evidenced during cold and dry periods because under these conditions microbial degradation is less effective than under warm and wet climatic conditions (low CPI values) (e.g., Kuder and Kruge, 1998; Xie et al., 2004; Rao et al., 2009). However, higher CPI values have also been related with warm temperatures and higher OM content (Brincat et al., 2000; Sachse et al., 2004; Jambrina-Enríquez et al., 2016). If a relationship exists between ACL-CPI and aridity (cold and dry or warm and dry) we would expect to find higher ACL and CPI values during the sedimentation of SUs XXIII-XXI and XVII-XII (1st Euclidean cluster group), which exhibits the highest δD_{C29} and δD_{C31} values (high TIC and low TOC values). However, we found the lowest ACL and CPI values in these SUs, which would suggest climate deterioration and low vegetation cover in the CS surroundings. These results fit well with previous findings that reported low CPI and ACL values during periods of low OM production (e.g., Brincat et al., 2000; Sachse et al., 2004; Castañeda et al., 2009; Jambrina-Enríquez et al., 2016).

δD values within each *n*-alkane homologue are correlated at a significant level ($p < 0.05$) with negative correlation coefficients ($R > -0.6$). Highly significant correlations were found within δD values of C_{29} and C_{31} ($R = 0.97$, $p < 0.05$) and between δD_{C29}, δD_{C31} and the TIC content ($R = 0.6$, $p < 0.05$), suggesting a common source

Table 1
Correlation indices for the hydrogen isotopes of every individual *n*-alkane, cumulative concentration of long-chained odd *n*-alkanes ($ACL_{29+31+33}$), their individual concentrations, and the total inorganic carbon (TIC) (N = 42). Significance was set at $p < 0.05$.

	δD_{C31}	$ACL_{29+31+33}$	nC_{29}	nC_{31}	TIC
δD_{C29}	R = 0.965 p = 8.301E-25	R = −0.431 p = 0.00441	R = −0.588 p = 0.0000426	R = −0.655 p = 0.0000025	R = 0.626 p = 0.000012
δD_{C31}		R = −0.407 p = 0.0075	R = −0.613 p = 0.0000158	R = −0.678 p = 0.000000828	R = 0.595 p = 0.0000409
$ACL_{29+31+33}$			R = 0.177 p = 0.262	R = 0.395 p = 0.00967	R = −0.318 p = 0.043
nC_{29}				R = 0.947 p = 2.059E-21	R = −0.562 p = 0.00013
nC_{31}					R = −0.595 p = 0.0000405

and precipitation amount or source as potential driving parameters for the hydrogen isotopic signal (Table 1). Indeed, recent $\delta^{18}O$ and δD studies on modern precipitation (March 2017–February 2018) in Montenegro (Podgorica) identified seasonal variations, with more negative values in winter (mean value $\delta D = -34‰$) when the temperature was the lowest and the amount of precipitation was very high under the influence of air masses originating from the Mediterranean, and less negative values (mean value $\delta D = -28‰$) in summer under the influence of Atlantic air masses (Živković et al., 2020). Similar seasonal δD variations were estimated with the OIPC model (Bowen and Revenaugh, 2003). In temperate regions the δD values from plant (leaf) water is controlled by δD precipitation values, which is mainly determined by air temperature and moisture source region (Dansgaard, 1964; Sachse et al., 2012; Kahmen et al., 2013). Thus, we assume that not only a decrease in air temperature but also changes in the moisture source region and/or changes in temperature at the moisture region may have been dominant drivers of the *n*-alkane hydrogen variability observed in the CS sequence.

On the other hand, there is an influence of the distribution of C_3 and C_4 plants on the hydrogen isotopic variability due to the different photosynthetic pathways with most D-depleted values in C_3 plants compared to C_4 plants (Gamarra et al., 2016). Moreover, shrubs and trees are most D-enriched than graminoids (Sachse et al., 2012). Based on archaeobotanical data (Shaw, 2017), the vegetation in CS is composed of C_3-plant types. If nC_{31} is dominant in grasses, then the most negative δD_{C29} and δD_{C31} (~−290‰) in 3rd Euclidean cluster group (XII-M2C, XX, XXIV and XXV) could be indicative of more graminoid input than in the 2nd Euclidean cluster group (XII-M2, XIX, XVIII, top of XXI, top of XXIV and XXVI/XXV boundary) (δD_{C29} and δD_{C31} ~−200‰); the highest δD_{C29} and δD_{C31} values (~−170‰) in the 1st Euclidean cluster group (X, XIII, XVII and XXI-XXII), with nC_{29} as dominant, are indicative of woody plant contribution. However, the archaeobotanical, zooarchaeological, micromorphological, archaeomagnetic and geochemical data discussed in the previous section suggest nC_{31} contribution in SUs XXIV and XX from woody taxa adapted to humid and cold conditions rather than grasses. Nevertheless, in XII-M2C we cannot rule out the input of grasses to the mixture with woody taxa adapted to humid conditions due to the limited complementary proxies obtained from this SU.

6.4. Past precipitation changes from sedimentary n-alkane D/H ratios

Based on the combination of elemental geochemistry and *n*-alkanes stable isotope proxies, we identified three main palaeoenvironmental stages of overall enhanced Mediterranean sourced precipitation. Humid periods are characterized by the most negative δD_{C29} and δD_{C31} (~−290‰) and lower TIC and higher TOC values (SUs XXV-XXIV and XX, and a single event XII_M2C), alternating with moderate humid conditions characterized by less negative δD_{C29} and δD_{C31} (~−200‰) and higher TIC and relatively higher TOC values (XXVI/XXV boundary, top of the XXIV, XIX-XVIII, XII-M2 and XI), and less humid stages with more positive δD_{C29} and δD_{C31} values (~−170‰) and higher TIC and lower TOC values (SUs XXIII-XXI, XVII-XIII and X) (Fig. 5).

After the moderate humid stage (SU XXVI/XXV boundary) identified within the 2nd Euclidean cluster group, the sedimentary proxies from SU XXV to the base of XXIV (lower δD_{C29} and δD_{C31} values and TIC content, but higher TOC, identified within the 3rd Euclidean cluster group) reveal a sharp increase in humidity and subsequently, a gradual shift to less humid conditions at the top of SU XXIV (2nd Euclidean cluster group: less negative δD_{C29} and δD_{C31} values and higher TIC content but relatively higher TOC) (Fig. 5).

The most negative δD_{C29} and δD_{C31} values correspond both natural (coarse gravels) and anthropogenic (black and white layers) sediments (SUs XXIV, XX, XVIII and XII-M2C), except for the positive δD_{C29} and δD_{C31} values in the SUs XXII (natural and anthropogenic sediments). As mentioned in the previous section, black layers from SUs XXIV, XXII, XX, XVIII and XII-M2C (combustion features) exhibit a strong odd-over-even carbon chain predominance indicating low-temperature combustion (≤300 °C, Mallol et al., 2013; Aldeias et al., 2016; Buonasera et al., 2019). Wang et al. (2017) reported that combustion at temperatures ≤300 °C under oxygen-free conditions results in a D-enrichment of δD by < 10‰ in long-chain alkanes relative to the original hydrogen isotopic composition. Similarly, combustion experiments performed by Connolly et al. (2021) under limited-oxygen conditions, which represent real conditions in archaeological contexts (combustion processes are not produced in oxygen-free conditions), demonstrated D-enrichment of δD by < 7‰ in long-chain alkanes relative to the original hydrogen isotopic signature up to 350 °C, and D-enrichment of δD by ~35‰ at 450 °C. Thus, thermal alteration in combustion substrates (black layers) do not alter the original hydrogen isotope signatures to a significant degree and may convey and report past hydroclimate information. On the other hand, white layers from combustion features in SUs XXIV, XX and XXII reported a strong odd-over-even carbon chain predominance with nC_{31} (SUs XXIV and XX) and nC_{29} (SU XXII) as dominant *n*-alkanes (low-temperature combustion), and negative (SUs XXIV and XX) and positive (SU XXII) δD_{C29} and δD_{C31} values. In view of all of the above, if the well preserved OM in the white layers represents the charred ground beneath the fire (meanly leaves), the combustion temperature was ≤350 °C and the long-chain alkanes preserve the original hydrogen isotopic signature. If this charred OM represent the charred wood fuel, the good state of OM preservation suggests incomplete combustion and temperatures ≤150 °C. Combustion of branches under limited oxygen conditions results in D-enrichment of δD by < 10‰ in long-chain alkanes relative to the original hydrogen isotopic composition up to 150 °C (Connolly et al., 2021). At 250 °C the combustion under limited-oxygen conditions in wood samples result in a loss of the primary *n*-alkane pattern (an even-over-odd *n*-alkane predominance) (Jambrina-Enríquez et al., 2018) and D-enrichment of δD by ~80‰. Thus, the δD values in the CS white layers preserve the primary hydrogen isotope signatures.

Fluctuations in TIC (carbonate) are covariant with the most negative δD_{C29} and δD_{C31} values at the basal units and increase up to the top in XXIV. Archaeomagnetic and magnetic fabric data from the SU XXIV combustion features suggest water-lain sedimentation processes (freezing and thawing processes with gelifluction) (Bradák et al., 2021). These findings agree with our isotopic and elemental analysis, which reveal a dominant humid stage during the deposition of SU XXIV (δD ~−290‰, 3rd Euclidean cluster group). Climatic deterioration at the top of SU XXIV (δD ~−200‰, 2nd Euclidean cluster group) culminates with the deposition of SUs XXIII-XXI, which exhibit the highest δD_{C29} and δD_{C31} values (δD ~−170‰, 1st Euclidean cluster group) indicative of less humid conditions and a transitional or moderated humid SU XXI (2nd Euclidean cluster group) (Fig. 5). With the sedimentation of SU XX, a return to more humid conditions is recorded (3rd Euclidean cluster group). As in SU XXIV, this unit exhibits several combustion features (three white layers and three black layers) indicative of human occupation but not as intensive as in SU XXIV. In fact, the sedimentation of combustion features is not as recurrent as in SU XXIV and is interrupted and intercalated by the deposition of coarse gravels. After this second humid stage, there is decreasing humidity up to the top of the sequence (2nd Euclidean cluster group), more intense in SUs XVII-XIII and X (1st Euclidean cluster group) and interrupted by a single humid event at SU XII-M2C (3rd Euclidean cluster group) and the transitional SU XII-M2. However, as mentioned in the previous section, we can rule out that the lowest δD_{C29} and δD_{C31} values in SU XII-M2C could also result from a mixture of grasses and woody plants.

δD_{C29} and δD_{C31} fluctuations along the CS sequence possibly indicate a change in the rain season: From a predominance of autumn-winter rainy months under the influence of Mediterranean air masses during the deposition of SUs XXV-XXIV, XX, XIX-XVIII, XII-XI to a predominance of late spring-summer rainy months influenced by Atlantic air masses from the SUs XXIII to XXI XVII-XIII, and X. On the other hand, the lowest δD values recorded in SUs XXV-XXIV and XX could suggest a cold-temperate (and humid) stage whereby a decrease in air temperature would lead to an isotopic depletion in precipitation (Dansgaard, 1964), and the increase of TOC could reflect the anthropogenic input of OM rather than a shift to more favourable climatic conditions linked to expansion of the vegetation cover around the site. This agrees with the findings of freezing and thawing processes in SU XXIV (Bradák et al., 2021).

6.5. Paleoevironmental conditions and chronology of the CS sequence, a general overview

Crvena Stijena offers one of the longest Middle Palaeolithic sequences spanning the last ~79 ka (78-52 ka, Unit XXIV, Mercier et al., 2017). Previous paleoenvironmental studies based on sedimentological and geochemical analysis (Brunnacker, 1975; SUs XXXI-I, MIS 6-Holocene) suggested warm and wet conditions during MIS 5e (SU XXIV), MIS 5a and MIS 5c (SUs XXIII-XVII) and the Holocene (SUs IV-I) based on carbonate dissolution, and dry and cold climatic conditions in SU XXV and above SU XVII based on good carbonate preservation. Later, high-resolution sampling and subsequent analyses of sedimentological, chemical, and magnetic properties (Morley, 2017) provided a more detailed paleoenvironmental interpretation along with new absolute chronometric dates that allowed for the following hypothesis (Mercier et al., 2017): Wet and warm climatic conditions associated with carbonate dissolution and periods of intense human occupation at the top of XXIV, XXI-XIX, and XVI-XIV, and dry and cold climatic conditions associated with carbonate preservation in SUs XXV, the base of XXIV, XXIII-XXII and XVIII-XVII. In this hypothesis, SU XXIV was correlated with the MIS 5a/4 boundary, XXIII-XIV with MIS 4, XIII-XI with MIS 3 (US XI was identified as Y-5 Campanian Ignimbrite, marking the 39.0 ka event, Morley and Woodward, 2011) and X with MIS 2 (Morley, 2017).

Our molecular and isotopic results correlate well with the humid and dry stages previously identified by Brunnacker (1975) and Morley (2017) with some discrepancies. Both SU XXIV and XX represent wet conditions and XXIII-XXI less humid conditions and Mediterranean *vs*. Atlantic sourced precipitation, respectively. However, above SU XX and up to X our data do not fit exactly with the previous findings. Climate deterioration toward less humid conditions and Atlantic sourced precipitation is recorded from SUs XIX to X (more evident in SUs XVII-XIII and X), and a potential wet event in SU XII-M2C (and transitional XII_M2) (Fig. 5).

We have identified two cold and dry phases and three temperate and wet phases that we tentatively correlated with cold/warm pulses recorded in the $\delta^{18}O$ record of the NGRIP ice core within MIS 3 (North Greenland Ice Core Project Members, 2004) (Fig. 5). Given the small number of dates below SU XIII and the uncertainty of the available dates, SUs XXVI-XXIV could be correlated with the Greenland Stadial G17/Greenland Interstadial 16 (GS17/GI16) transition, a warm and wet phase, with a low temperature pulse in SU XXV and the base of XXIV (cold-temperate and wet). The first cold and arid phase (XXIII-XXI) could be tentatively correlated with GS15 (~54.3 ka BP, Svensson et al., 2008) which preceded the GI14 (SUs XXI-XX-XVIII, cold to warm-temperate and wet phase). The second cold and arid phase (SUs XVII-XIII_XII-M2C1) could be tentatively correlated with GS13, coinciding with HE5 which preceded GI12 (SU XII-M2C-XI, cold to warm-temperate and wet phase). This paleoenvironmental model fits well with the faunal model (MIS4 in SUs XXVI-XXV, MIS3 in SUs XXIV-XII and MIS2 in SU X; Morin and Soulier, 2017) and is supported by the AMS data from SUs XII (M2C/C1, 43.7−54.4 Ka cal BP) and XIII (M3, 45.3−54.9 Ka cal BP) and OSL data of SUs XII (37.6 ± 2.9−43.2 ± 3.7 Ka) and XIII (44.2 ± 3.4 Ka), as well as the youngest ESR data of SU XX (48.3 ± 2.4 Ka) and TL data from SU XXIV (52.2 ± 6.6 Ka) that places SUs XII-XXIV within MIS 3 (Fig. 5). Although the archaeological assemblages (Mousterian points and retouched Levallois flakes, Mihailović and Whallon, 2017a) combined with geological, faunal and wood charcoal data correlate the upper part of the CS sequence (XIII-XI) with MIS 3, the chronology of the lower part of the sequence is uncertain considering the oldest TL data in SU XX (65.5 ± 14 Ka) and in SU XXIV (TL: 70.0 ± 6.2 ka and ESR: 78.3 ± 0.3 ka), which place these layers in MIS 4 and MIS 5a, respectively.

Interstadial conditions in Europe are characterized by warming and increase in humidity, while stadial climatic conditions are associated with cooling and decrease in humidity (e.g., Voelker, 2002; van Meerbeeck et al., 2011; Agosta and Compagnucci, 2016). Substantial increase in precipitation during GIs have been related with an increase of winter precipitation and an increase of deciduous woody taxa (*Quercus*, *Abies* and *Fagus*) in Lake Ordhir (Lézine et al., 2010), Lake Prespa (Panagiotopoulos et al., 2014) and Lake Monticchio (Italy, Allen et al., 1999). These findings agree with our low δD_{C29} and δD_{C31} values (high CPI, ACL and TOC values, nC_{31} as tree-derived alkane, 2nd Euclidean cluster groups) and the predominance of autumn-winter rainy months under the influence of Mediterranean air masses which would favour and increase of the vegetation cover (Mediterranean forest) in the CS area (Fig. 5). Our humid and relatively cold-temperate climatic conditions correspond with the levels of intense human occupation in the CS rock shelter (3rd Euclidean cluster group) and agree with the faunal spectrum from SUs XXVI and XXIV (Bos/Bison, Equus ferus caballus, Stephanorhinus/Coelodonta) (Morin and Soulier, 2017), the cool-wet-adapted plant taxa (Shaw, 2017) and freezing and thawing processes (Bradák et al., 2021) identified in SU XXIV. Cold and arid phases (high δD_{C29} and δD_{C31}, low CPI, ACL and TOC values, nC_{29} as tree-derived alkanes, 1st Euclidean cluster group) possibly reduced the Mediterranean-tree cover allowing the presence of crioromediterranean tree species (e.g., *Pinus sylvestris*).

Despite the dating uncertainties, some correlation could be attempted with Middle Palaeolithic sites in the northern Balkans (i.e., Mujina Pećina, 49 and ~39 cal ka, Boschian et al., 2017). At Mujina Pećina, human occupation was more intense during the cold/arid Heinrich Event 5 (HE5), and more sporadic after HE5 (during a warm but environmental unstable phase), with two Mousterian hearths (~45 - 43 Ka) found in layers associated with cold or fresh conditions where freezing and thawing processes have been identified (Boschian et al., 2017). Human occupation levels in Mujina Pećina could be tentatively correlated with the human occupation recorded in CS SU XVII-XII_M2C1 during cold and dry conditions (HE5) and under cold-temperate and wet conditions (SU XII_M2C, 47.7–48.8 Ka). Since the studied CS sequence spans from MIS 4/3, the most intense occupation in CS (SUs XXIV and XX) has been related with humid (and tentatively cold-temperate) climatic conditions.

7. Conclusions

Our compound-specific hydrogen (δD_{C29} and δD_{C31}) leaf wax (i.e., *n*-alkanes) study of a 7 m-deep sedimentary sequence in the Crvena Stijena Middle Paleolithic site has shed light on paleohydrological variability and climate/human interaction. Agglomerative hierarchical clustering and principal component analysis of our data show three different groups, which have been related with hydroclimate changes:

i) Units X (13.6–28.5 Ka), XIII-XVII (XIII: 49.3 Ka) and XXI-XXIII were deposited under dry (and tentatively cold) conditions and Atlantic sourced precipitation. OM preservation is relatively low (CPI~2). These SUs recorded few or relatively few (XV, XVII, XXI, XXIII) and moderate (XIII, XVI) artifacts, except for SUs XXII (numerous artifacts and remain of fauna, occasional combustion features composed by white and/or grey ash layer and their underlying black or dark brown, charcoal-rich thermally altered layer) and XIV (numerous artifacts) (Mihailović et al., 2017a,b).

ii) Units XI (39 Ka, Y5 tephra layer), XII_M2, XVIII-XIX, top of XXI, top of XXIV (78.3–52.2 Ka) and XXVI, were deposited during relatively humid conditions (and tentatively warm-temperate conditions) and Mediterranean sourced precipitation. OM is well preserved (CPI >5). These SUs recorded few (XI, XXI, XXVI) and relatively few (M2) artifacts except for SU XVIII (numerous artifacts and remain of fauna, no distinct white and black combustion layers) (Mihailović et al., 2017a,b).

iii) Units XII-M2C (48 - 47 Ka), XX (65.5–48.3 Ka) and base of XXIV-XXV (78.3–52.2 Ka), related with humid (and tentatively cold-temperate) conditions and Mediterranean sourced precipitation. OM is well preserved in the anthropogenic layers (CPI~4). Comparison with experimental fire data (e.g., Mallol et al., 2013; Jambrina-Enríquez et al., 2018) suggests that combustion temperatures were <350 °C and thus preserve their original paleoprecipitation signal (Connolly et al., 2021). These SUs recorded human occupation layers with numerous artifacts and hearth (M2C) and numerous artifacts and remain of fauna as well as distinct combustion features (white and black layers) (XX and XXIV) except for SU XXV (few artifacts) (Mihailović et al., 2017a,b).

Our molecular and compound specific stable hydrogen isotope ratios in long chain *n*-alkanes bracket the CS sequence between the MIS 4/3 boundary (SU XXVI/XXV) and MIS 3 (SUs XXV-X). Despite chronometric uncertainty based on the available dates, we tentatively correlated our data with specific warm/cold phases in the $\delta^{18}O$ record of the NGRIP ice core (North Greenland Ice Core Project Members, 2004), lake pollen sequences (Lake Ohrid, Lézine et al., 2010; Lake Prespa, Panagiotopoulos et al., 2014; Lake Monticchio, Allen et al., 1999), and geological (Morley, 2017), faunal (Morin and Soulier, 2017) and palaeobotanical (charcoal, Shaw, 2017) age-models previously proposed for CS (Whallon and Morin, 2017). Our results indicate at least three aridity trends between MIS 4/3 (SU XXV) and MIS 3 (SU XI): i) from SU XXV to XXI (52.2/78.3 to 48.3/65.5 Ka), ii) from SU XX to XII-M2C1 (48.3/65.5 to 49.3 Ka) and ii) from SU XII-M2C to SU XI (48–39 Ka). The robust available dates from the upper part of the CS sequence (SUs XIII-XI; MIS3) allowed us to correlate the dry (and tentatively cold) stage identified in SU XIII with HE5. The layers representing intense human occupation in CS (i.e., base of SU XXIV, SUs XX and XII-M2C) are associated with humid and tentatively cold-temperate conditions during MIS 3. SUXII-M2C (47.7–48.8 Ka) could be tentatively correlated with the human occupations associated with cold or cool conditions recorded in Mujina Pećina (northern Balkans) at ~45 - 43 Ka.

Our molecular and compound-specific hydrogen isotope dataset contributes a more accurate paleoenvironmental reconstruction for CS and brings us closer to the local climatic conditions that prevailed during the Middle Paleolithic human occupations recorded at the site. This new dataset also addresses past hydrological variability in a region that is sensitive to short-lived climatic shifts (i.e., the Balkan peninsula) and overall, in the Mediterranean region during the last glacial/interglacial cycle.

Author contributions statement

Margarita Jambrina-Enríquez: Conceptualization; Investigation; Formal analysis; Writing – original draft. **Carolina Mallol:** Conceptualization; Resources; Writing - review and editing. **Gilbert Tostevin and Gilliane Monnier:** Funding acquisition; Project administration, Writing - review & editing. **Goran Pajović, Nikola Borovinić and Mile Baković:** Project administration.

Declaration of competing interest

The authors declare that they have no known competing financial interests or personal relationships that could have appeared to influence the work reported in this paper.

Data availability

I have shared the link to my data at the Attach File step

Acknowledgements

Financial support for research at Crvena Stijena was provided by the United States National Science Foundation (BCS 1758285, https://www.nsf.gov/), the University of Minnesota Grant-in-Aid of Research (https://research.umn.edu/funding-awards/ovpr-funding/grant-aid), and the National Museum and Ministry of

Culture of Montenegro. We thank Dr. Antonio V. Herrera-Herrera (AMBI Lab) for his collaboration in this research, Rory Connolly for assistance in the field sampling, and the entire Crvena Stijena excavation team for facilitating this research. We thank the villagers of Petrovići for their immense hospitality.

Appendix A. Supplementary data

Supplementary data to this article can be found online at https://doi.org/10.1016/j.quascirev.2022.107771.

References

Agosta, E.A., Compagnucci, R.H., 2016. Abrupt climate changes during the marine isotope stage 3 (MIS 3). In: Gasparini, G., Rabassa, J., Deschamps, C., Tonni, E. (Eds.), Marine Isotope Stage 3 in Southern South America, 60 KA B.P.-30 KA B.P. Springer Earth System Sciences. Springer, Cham, pp. 81–106. https://doi.org/10.1007/978-3-319-40000-6_5.

Aldeias, V., Dibble, H.L., Sandgathe, D., Goldberg, P., McPherron, S.J., 2016. How heat alters underlying deposits and implications for archaeological fire features: a controlled experiment. J. Archaeol. Sci. 67, 64–79. https://doi.org/10.1016/j.jas.2016.01.016.

Alexandrov, A.H., Andonovski, V., 2011. EUFORGEN Technical Guidelines for Genetic Conservation and Use of Macedonian Pine (Pinus Peuce). Bioversity International, Rome, Italy.

Allen, J.R.M., Brandt, U., Brauer, A., Hubberten, H.W., Huntley, B., Keller, J., Kraml, M., Mackensen, A., Mingram, J., Negendank, J.F.W., Nowaczyk, N.R., Oberhänsli, H., Watts, W.A., Wulf, S., Zolitschka, B., 1999. Rapid environmental changes in southern Europe during the last glacial period. Nature 400, 740–743. https://doi.org/10.1038/23432.

Baković, M., Mihailović, B., Mihailović, D., Morley, M., Vušović-lučić, Z., Whallon, R., Woodward, J., 2009. Crvena Stijena excavations 2004-2006, preliminary report. Eurasian Prehistory 6, 3–31.

Basler, D. (Ed.), 1975. Crvena Stijena: Zbornik Radova. Zajednica Kulturnih Ustanova, Nikšiæ.

Benazzi, S., Douka, K., Fornai, C., Bauer, C., Kullmer, O., Svoboda, J., Pap, I., Mallegni, F., Bayle, P., Coquerelle, M., Condemi, S., Ronchitelli, A., Harvati, K., Weber, G., 2011. Early dispersal of modern humans in Europe and implications for neanderthal behaviour. Nature 479, 525–528. https://doi.org/10.1038/nature10617.

Biltekin, D., Burjachs, F., Vallverdú, J., Sharp, W.D., Mertz-Kraus, R., Chacón, M.G., Saladié, P., Bischoff, J.L., Carbonell, E., 2019. Vegetation and climate record from abric Romaní (Capellades, northeast Iberia) during the upper Pleistocene (MIS 5d–3). Quat. Sci. Rev. 220, 154–164. https://doi.org/10.1016/j.quascirev.2019.07.035.

Boschian, G., Gerometta, K., Ellwood, B.B., Karavanic, I., 2017. Late Neandertals in Dalmatia: site formation processes, chronology, climate change and human activity at Mujina Pecina, Croatia. Quat. Int. 450, 12–35. https://doi.org/10.1016/j.quaint.2016.09.066.

Bowen, G.J., Revenaugh, J., 2003. Interpolating the isotopic composition of modern meteoric precipitation. Water Resour. Res. 39 (10), 1299. https://doi:10.129/2003WR002086.

Braadbaart, F., Poole, I., 2008. Morphological, chemical and physical changes during charcoalification of wood and its relevance to archaeological contexts. J. Archaeol. Sci. 35 (9), 2434–2445. https://doi.org/10.1016/j.jas.2008.03.016.

Bradák, B., Carrancho, A., Herrejón, A., Villalaín, J.J., Monnier, J.G., Tostevin, G., Mallol, C., Pajovic, G., Baković, M., Borovinić, N., 2021. Magnetic fabric and archaeomagnetic analyses of anthropogenic ash horizons in a cave sediment succession (Crvena Stijena site, Montenegro). Geophys. J. Int. 224, 795–812. https://doi.org/10.1093/gji/ggaa461.

Bray, E.E., Evans, E.D., 1961. Distribution of n-paraffins as a clue to recognition of source beds. Geochem. Cosmochim. Acta 22, 2–15. https://doi.org/10.1016/0016-7037/61)90069-2.

Buonasera, T., Herrera-Herrera, A.V., Mallol, C., 2019. Experimentally derived sedimentary, molecular, and isotopic characteristics of bone-fueled hearths. J. Archaeol. Method Theor. 26 (4), 1327–1375. https://doi.org/10.1007/s10816-019-09411-3.

Brincat, D., Yamada, K., Ishiwatari, R., Uemura, H., Naraoka, H., 2000. Molecular-isotopic stratigraphy of long-chain n-alkanes in Lake Baikal Holocene and glacial age sediments. Org. Geochem. 31, 287. https://doi.org/10.1016/S0146-6380(99)00164-3.

Brunnacker, K., 1975. Die sedimente der Crvena Stijena. In: Basler, Đ. (Ed.), Crvena Stijena – Zbornik Radova. Nikšić, Zajednica Kulturnih Ustanova, pp. 171–203.

Burić, D., Ducić, V., Mihajlović, J., 2014a. The Climate of Montenegro: Modificators and Types – Part Two. Bulletin of the Serbian Geographical Society. https://doi.org/10.2298/GSGD1401073B. Tome XCIV - No 1.

Burić, D., Ducić, V., Mihajlović, Luković J., Dragojlović, J., 2014b. Relationship between the precipitation variability in Montenegro and the Mediterranean oscillation. Tome XCIV No 4. https://doi.org/10.2298/GSGD1404109B.

Bush, R.T., McInerney, F.A., 2013. Leaf wax n-alkane distributions in and across modern plants: implications for paleoecology and chemotaxonomy. Geochem. Cosmochim. Acta 117, 161–179. https://doi.org/10.1016/j.gca.2013.04.016.

Bush, R.T., McInerney, F.A., 2015. Influence of temperature and C_4 abundance on n-alkane chain length distributions across the central USA. Org. Geochem. 79, 65–73. https://doi.org/10.1016/j.orggeochem.2014.12.003.

Castañeda, I.S., Werne, J.P., Johnson, T.C., Filley, T.R., 2009. Late Quaternary vegetation history of southeast Africa: the molecular isotopic record from Lake Malawi. Palaeogeogr. Palaeoclimatol. Palaeoecol. 275, 100–112. https://doi.org/10.1016/j.palaeo.2009.02.008.

Cohen, K.M., Gibbard, P.L., 2019. Global chronostratigraphical correlation table for the last 2.7 million years. Quat. Int. 500, 20–31. https://doi.org/10.1016/j.quaint.2019.03.009.

Collins, J.A., Schefuß, E., Mulitza, S., Prange, M., Werner, M., Tharammal, T., Paul, A., Wefer, G., 2013. Estimating the hydrogen isotopic composition of past precipitation using leaf-waxes from western Africa. Quat. Sci. Rev. 65, 88–101. https://doi.org/10.1016/j.quascirev.2013.01.007.

Columbu, A., Chiarini, V., Spötl, C., Benazi, S., Hellstrom, J., Cheng, H., De Waele, J., 2020. Speleothem record attests to stable environmental conditions during Neanderthal–modern human turnover in southern Italy. Nat. Ecol. Evol. 4, 1188–1195. https://doi.org/10.1038/s41559-020-1243-1.

Connolly, R., Jambrina-Enríquez, M., Herrera-Herrera, A.V., Vidal-Matutano, P., Fagoaga, A., Marquina-Blasco, R., Marin-Monfort, M.D., Ruiz-Sánchez, F.J., Laplana, C., Bailon, S., Pérez, L., Leierer, L., Hernández, C.M., Galván, B., Mallol, C., 2019. A multiproxy record of palaeoenvironmental conditions at the Middle Palaeolithic site of Abric del Pastor (Eastern Iberia). Quat. Sci. Rev. 225, 106023. https://doi.org/10.1016/j.quascirev.2019.106023.

Connolly, R., Jambrina-Enríquez, M., Herrera-Herrera, A.V., Mallol, C., 2021. Investigating hydrogen isotope variation during heating of n-alkanes under limited oxygen conditions: implications for Palaeoclimate reconstruction in archaeological settings. Molecules 26, 1830. https://doi.org/10.3390/molecules26071830.

Courty, M.A., Vallverdu, J., 2001. The microstratigraphic record of abrupt climate changes in cave sediments of the Western Mediterranean. Geoarchaeol. Int. J. 16 (5), 467–499. https://doi.org/10.1002/gea.1002.

Cranwell, P., 1981. Diagenesis of free and bound lipids in terrestrial detritus deposited in a lacustrine sediment. Org. Geochem. 3, 79–89. https://doi.org/10.1016/0146-6380(81)90002-4.

Cranwell, P.A., Eglinton, G., Robinson, N., 1987. Lipids of aquatic organisms as potential contributors to lacustrine sediments-II. Org. Geochem. 11, 513–527. https://doi.org/10.1016/0146-6380(87)90007-6.

Ćulafić, S., Vuksanović, S., Bubanja, N., Polović, L., Čađenović, N., Dragićević, S., Malidžan, S., Burzanović, K., Vizi, A., Biberdžić, V., Ćetković, I., Karaman, M., 2017. Ecological context the surroundings of Crvena Stijena. In: Whallon, Robert (Ed.), Crvena Stijena in Cultural and Ecological Context Multidisciplinary Archaeological Research in Montenegro, pp. 28–45.

d'Errico, F., Goñi, M.F.S., 2003. Neandertal extinction and the millennial scale climatic variability of OIS 3. Quat. Sci. Rev. 22 (8–9), 769–788. https://doi.org/10.1016/S0277-3791(03)00009-X.

Dansgaard, W., 1964. Stable isotopes in precipitation. Tellus 16 (4), 436–468. https://doi.org/10.1111/j.2153-3490.1964.tb00181.x.

Dansgaard, W., Johnsen, S.J., Clausen, H.B., Dahl-Jensen, D., Gundestrup, N.S., Hammer, C.U., et al., 1993. Evidence for general instability of past climate from a 250-kyr ice-core record. Nature 364 (6434), 218–220.

Diefendorf, A., Freeman, K.H., Heather, G.V., 2011. Production of n-alkyl lipids in living plants and implications for the geologic past. Geochim. Cosmochim. Acta 75 (23), 7472–7485. https://doi.org/10.1016/j.gca.2011.09.028.

Diefendorf, A.F., Sberna, D.T., Taylor, D.W., 2015a. Effect of thermal maturation on plant-derived terpenoids and leaf wax n-alkyl components. Org. Geochem. 89–90, 61–70. https://doi.org/10.1016/j.orggeochem.2015.10.006.

Diefendorf, A.F., Leslie, A.B., Wing, S.L., 2015b. Leaf wax composition and carbon isotopes vary among major conifer groups. Geochim. Cosmochim. Acta 170, 145–156. https://doi.org/10.1016/j.gca.2015.08.018.

Dodd, R.S., Poveda, M.M., 2003. Environmental gradients and population divergence contribute to variation in cuticular wax composition in Juniperus communis. Biochem. Systemat. Ecol. 31, 1257–1270. https://doi.org/10.1016/S0305-1978(03)00031-0.

Eglinton, G., Hamilton, R.J., 1967. Leaf epicuticular waxes. Science 156 (3780), 1322–1335. https://doi.org/10.1126/science.156.3780.1322.

Ficken, K.J., Li, B., Swain, D.L., Eglinton, G., 2000. An n-alkane proxy for the sedimentary input of submerged/floating freshwater aquatic macrophytes. Org. Geochem. 31, 745–749. https://doi.org/10.1016/S0146-6380(00)00081-4.

Gamarra, B., Sachse, D., Kahmen, A., 2016. Effects of leaf water evaporative ^{2}H-enrichment and biosynthetic fractionation on leaf wax n-alkane δ^2H values in C_3 and C_4 grasses. Plant Cell Environ. 39, 2390–2403. https://doi.org/10.1111/pce.12789.

García-Alix, A., Camuera, J., Ramos-Román, M.J., Toney, J.L., Sachse, D., Schefuß, E., Jiménez-Moreno, G., Jiménez-Espejo, F.J., López-Avilés, A., Anderson, R.S., Yanes, Y., 2021. Paleohydrological dynamics in the Western Mediterranean during the last glacial cycle. Global Planet. Change 202, 103527. https://doi.org/10.1016/j.gloplacha.2021.103527.

Gilligan, I., 2007. Neanderthal extinction and modern human behaviour: the role of climate change and clothing. World Archaeol. 39 (4), 499–514. https://doi.org/10.1080/00438240701680492.

Goldberg, P., Miller, C.E., Schiegl, S., Ligouis, B., Berna, F., Conard, N.J., Wadely, L., 2009. Bedding, hearths, and site maintenance in the Middle Stone age of Sibudu cave, KwaZulu-Natal, South Africa. Archaeol. Anthropol. Sci. 1, 95–122. https://

doi.org/10.1007/s12520-009-0008-1.
Gutiérrez, 1990. Dendrocronología de Pinus sylvestris L. en Cataluña. Orsis 5, 23–41.
Hedges, J.I., Prahl, F.G., 1993. Early diagenesis: consequences for applications of molecular biomarkers. In: Engel, M.H., Macko, S.A. (Eds.), Organic Geochemistry. Principles and Applications. Plenum Press, New York, pp. 237–253.
Heinrich, H., 1988. Origin and consequences of cyclic ice rafting in the northeast Atlantic Ocean during the past 130,000 years. Quat. Res. 29 (2), 142–152. https://doi.org/10.1016/0033-5894(88)90057-9.
Herrera-Herrera, A.V., Mohamed-Rodríguez, N., Socas-Rodríguez, B., Mallol, C., 2020. Development of a QuEChERS-based method combined with gas chromatography-mass spectrometry for the analysis of alkanes in sediments. Microchem. J. 155, 104774. https://doi.org/10.1016/j.microc.2020.104774.
Higham, T., Douka, K., Wood, R., Ramsey, C.B., Brock, F., Basell, L., et al., 2014. The timing and spatiotemporal patterning of Neanderthal disappearance. Nature 512 (7514), 306–309. https://doi.org/10.1038/nature13621.
Hoefs, M.J., Rijpstra, W.C., Sinninghe Damsté, J.S., 2002. The influence of oxic degradation on the sedimentary biomarker record I: evidence from Madeira Abyssal Plain turbidites. Geochim. Cosmochim. Acta 66, 2719–2735. https://doi.org/10.1016/S0016-7037(02)00864-5.
Hou, J., Tian, Q., Wang, M., 2018. Variable apparent hydrogen isotopic fractionation between sedimentary n-alkanes and precipitation on the Tibetan Plateau. Org. Geochem. 122, 78–86. https://doi.org/10.1016/j.orggeochem.2018.05.011.
Jambrina-Enríquez, M., Sachse, D., Valero-Garcés, B.L., 2016. A deglaciation and Holocene biomarker-based reconstruction of climate and environmental variability in NW Iberian Peninsula: the Sanabria Lake sequence. J. Paleolimnol. 56, 49–66. https://doi.org/10.1007/s10933-016-9890-6.
Jambrina-Enríquez, M., Herrera-Herrera, A.V., Mallol, C., 2018. Wax lipids in fresh and charred anatomical parts of the Celtis australis tree: insights on paleofire interpretation. Org. Geochem. 122, 147–160. https://doi.org/10.1016/j.orggeochem.2018.05.017.
Jambrina-Enríquez, M., Herrera-Herrera, A.V., de Vera, C.R., Leierer, L., Connolly, R., Mallol, C., 2019. n-Alkyl nitriles and compound-specific carbon isotope analysis of lipid combustion residues from Neanderthal and experimental hearths: identifying sources of organic compounds and combustion temperatures. Quat. Sci. Rev. 222, 105899. https://doi.org/10.1016/j.quascirev.2019.105899.
Jones, D.S., Monnier, G., Cooper, A., Baković, M., Pajović, G., Borovinić, N., Tostevin, G., 2021. Applying high-throughput rRNA gene sequencing to assess microbial contamination of a 40-year old exposed archaeological profile. J. Archaeol. Sci. 126, 105308.
Jouzel, J., Masson-Delmotte, V., Cattani, O., Dreyfus, G., Falourd, S., Hoffmann, G., Minster, B., Nouet, J., Barnola, J.M., Chappellaz, J., Fischer, H., Gallet, J.C., Johnsen, S., Leuenberger, M., Loulergue, L., Luethi, D., Oerter, H., Parrenin, F., Raisbeck, G., Raynaud, D., Schilt, A., Schwander, J., Selmo, E., Souchez, R., Spahni, R., Stauffer, B., Steffensen, J.P., Stenni, B., Stocker, T.F., Tison, J.L., Werner, M., Wolff, E.W., 2007. Orbital and millennial antarctic climate variability over the past 800,000 years. Science 317, 793–796. https://doi.org/10.1126/science.1141038.
Jovanović, B., Jovanović, R., Zupančić, M., 1986. Prirodna Potencijalna Vegetacija Jugoslavije (Komentar Karte M 1:1000.000). 18 Kongres IUFRO Yu 86. Ljubljna, p. 122.
Kahmen, A., Schefuß, E., Sachse, D., 2013. Leaf water deuterium enrichment shapes leaf wax n-alkane dD values of angiosperm plants I: experimental evidence and mechanistic insights. Geochim. Cosmochim. Acta . 111, 39–49. https://doi.org/10.1016/j.gca.2012.09.003.
Knicker, H., Hilscher, A., De la Rosa, J.M., González-Pérez, J.A., González-Vila, F.J., 2013. Modification of biomarkers in pyrogenic organic matter during the initial phase of charcoal biodegradation in soils. Geoderma 197, 43–50.
Kozłowski, J.K., 2004. Early upper Paleolithic Levallois-derived industries in the Balkans and in the middle Danube basin. Anthropologie 42 (3), 263–280.
Kuder, T., Kruge, M.A., 1998. Preservation of biomolecules in sub-fossil plants from raised peat bogs—a potential paleoenvironmental proxy. Org. Geochem. 29, 1355–1368. https://doi.org/10.1016/S0146-6380(98)00092-8.
Kuehn, D.D., Dickson, D.B., 1999. Stratigraphy and non-cultural site formation at the Shurmai rockshelter (GnJm1) in the Mukogodo Hills of north-Central Kenya. Geoarchaeology 14, 63–85.
Lambrecht, G., Rodríguez de Vera, C., Jambrina-Enríquez, M., Crevecoeur, I., Gonzalez-Urquijo, J., Lazuen, T., Monnier, G., Pajovic, G., Tostevin, G., Mallol, C., 2021. Characterisation of charred organic matter in micromorphological thin sections by means of Raman spectroscopy. Archaeol. Anthropol. Sci. 13, 13. https://doi.org/10.1007/s12520-020-01263-3.
Lang, N., Wolff, E.W., 2011. Interglacial and glacial variability from the last 800 ka in marine, ice and terrestrial archives. Clim. Past 7, 361–380. https://doi.org/10.5194/cp-7-361-2011.
Leierer, L., Jambrina-Enríquez, M., Herrera-Herrera, A.V., Connolly, R., Hernández, C.M., Galván, B., Mallol, C., 2019. Insights into the timing, intensity and natural setting of Neanderthal occupation from the geoarchaeological study of combustion structures: a micromorphological and biomarker investigation of El Salt, unit Xb, Alcoy, Spain. PLoS One 14 (4), e0214955. https://doi.org/10.1371/journal.pone.0214955.
Leroi-Gourhan, A., 1973. Séminaire sur les structures d'habitat: témoins de combustión. Collège de France, Paris.
Lézine, A.-M., von Grafenstein, U., Andersen, N., Belmecheri, S., Bordon, A., Caron, B., Cazet, J.-P., Erlenkeuser, H., Fouache, E., Grenier, C., Huntsman-Mapila, P., Hureau-Mazaudier, D., 2010. Lake Ohrid, Albania, provides an exceptional multi-proxy record of environmental changes during the last glacial–interglacial cycle. Palaeogeogr. Palaeoclimatol. Palaeoecol. 287 (1–4), 116–127. https://doi.org/10.1016/j.palaeo.2010.01.016.
Li, C., Ma, S., Xia, Y., He, X., Gao, W., Zhang, G., 2020. Assessment of the relationship between ACL/CPI values of long chain n-alkanes and climate for the application of paleoclimate over the Tibetan Plateau. Quat. Int. 544, 76–87. https://doi.org/10.1016/j.quaint.2020.02.028.
Mallol, C., Hernández, C.M., Cabanes, D., Sistiaga, A., Machado, J., Rodríguez, A., Pérez, L., Galván, B., 2013. The black layer of Middle Palaeolithic combustion structures. Interpretation and archaeostratigraphic implications. J. Archaeol. Sci. 40, 2515–2537. https://doi.org/10.1016/j.jas.2012.09.017.
Mallol, C., Mentzer, S., Miller, C., 2017. Combustion features. In: Nicosia, C., Stoops, G. (Eds.), Archaeological Soil and Sediment Micromorphology. Wiley, pp. 299–326.
Mallol, C., Hernández, C., Mercier, N., Falguères, C., Carrancho, A., Cabanes, D., Vidal-Matutano, P., Connolly, R., Pérez, L., Mayor, A., Ben Arous, E., Gaván, B., 2019. Fire and brief human occupations in Iberia during MIS 4: evidence from Abric del Pastor (Alcoy, Spain). Sci. Rep. 9, 18281. https://doi.org/10.1038/s41598-019-54305-9.
March, R.J., Whallon, R., Morley, M.W., 2017. Studying neanderthal fire structures from Crvena Stijena. In: Whallon, Robert (Ed.), Crvena Stijena in Cultural and Ecological Context Multidisciplinary Archaeological Research in Montenegro, pp. 340–450.
Mentzer, S.M., 2017. Rockshelter settings. In: Gilbert, A.S., Dordrecht, N.L. (Eds.), Encyclopedia of Geoarchaeology. Encyclopedia of Earth Sciences Series. Springer-Verlag. https://doi.org/10.1007/978-1-4020-4409-0_159.
Mercier, N., Rink, W.J., Rodrigues, K., Morley, M.W., Linden, M.V., Whallon, R., 2017. Radiometric dating of the Crvena Stijena sequence. In: Whallon, Robert (Ed.), Crvena Stijena in Cultural and Ecological Context Multidisciplinary Archaeological Research in Montenegro, pp. 140–150.
Meyer, M., Fu, Q., Aximu-Petri, A., Glocke, I., Nickel, B., Arsuaga, J.L., Martínez, I., Gracia, A., Carbonell, E., Pääbo, S., 2014. A Mitochondrial Genome Sequence of a Hominin from Sima de los Huesos. Nature 505, 403–406. https://doi.org/10.1038/nature12788.
Meyer, M., Arsuaga, J.L., de Filippo, C., Nagel, S., Aximu-Petri, A., Nickel, B., Martínez Mendizábal, I., Gracia Téllez, A., Bermúdez de Castro, J.M., Carbonell, E., Viola, B., Kelso, J., Prüfer, K., Pääbo, S., 2016. Nuclear DNA sequences from the Middle Pleistocene Sima de los Huesos hominins. Nature 531, 504–507. https://doi.org/10.1038/nature17405.
Meyers, P.A., Ishiwatari, R., 1993. Lacustrine organic geochemistry—an overview of indicators of organic matter sources and diagenesis in lake sediments. Org. Geochem. 20, 867–900. https://doi.org/10.1016/0146-6380(93)90100-P.
Mihailović, D., Whallon, R., 2017. Crvena Stijena revisited: the late Mousterian assemblages. Quat. Int. 450, 36–49. https://doi.org/10.1016/j.quaint.2016.12.026.
Mihailović, D., Mihailović, B., Whallon, R., 2017a. Excavations of middle Paleolithic - Mesolithic layers. In: Whallon, Robert (Ed.), Crvena Stijena in Cultural and Ecological Context Multidisciplinary Archaeological Research in Montenegro, pp. 150–204.
Mihailović, D., Mihailović, B., Borovinić, N., 2017b. Newer excavations - archaeological stratigraphy. In: Whallon, Robert (Ed.), Crvena Stijena in Cultural and Ecological Context Multidisciplinary Archaeological Research in Montenegro, pp. 132–139.
Miller, C.E., Goldberg, P., Berna, F., 2013. Geoarchaeological investigations at diepkloof rock shelter, western Cape, South Africa. J. Archaeol. Sci. 40 (9), 3432–3452. https://doi.org/10.1016/j.jas.2013.02.014.
Monnier, G., Tostevin, G., Pajović, G., Borovinić, N., Baković, M., 2020. Nova Istraživanja Paleolitskog Nalazišta Crvena Stijena. Istorijski Kontekst. Istorijski Zapisi, Godina XCIII, 1-2/2020, pp. 71–108.
Morin, E., Soulier, M.C., 2017. The Paleolithic faunal remains from Crvena Stijena. In: Whallon, Robert (Ed.), Crvena Stijena in Cultural and Ecological Context Multidisciplinary Archaeological Research in Montenegro, pp. 266–295.
Morley, M.W., 2007. Mediterranean Quaternary Rockshelter Sediment Records: A Multi-proxy Approach to Environmental Reconstruction (PhD thesis). University of Manchester.
Morley, M.W., 2017. The geoarchaeology of Crvena Stijena site formation processes, Palaeoenvironments and Hominin activity. In: Whallon, Robert (Ed.), Crvena Stijena in Cultural and Ecological Context Multidisciplinary Archaeological Research in Montenegro, pp. 82–132.
Morley, M., Woodward, J., 2011. The Campanian Ignimbrite (Y5) tephra at Crvena Stijena rockshelter, Montenegro. Quat. Res. 75 (3), 683–696. https://doi.org/10.1016/j.yqres.2011.02.005.
North Greenland Ice Core Project Members, 2004. High-resolution record of Northern Hemisphere climate extending into the last interglacial period. Nature 431, 147–151. https://doi.org/10.1038/nature02805.
North Greenland Ice Core Project Members, 2007. 50 year means of oxygen isotope data from ice core NGRIP. PANGAEA. https://doi.org/10.1594/PANGAEA.586886.
O'Malley, V.P., Burke, R.A., Schlotzhauer, W.S., 1997. Using GC-MS/Combustion/IRMS to determine the 13C/12C ratios of individual hydrocarbons produced from the combustion of biomass materials—application to biomass burning. Org. Geochem. 27, 567–581. https://doi.org/10.1016/S0146-6380(97)00087-9.
Panagiotopoulos, K., Böhm, A., Leng, M.J., Wagner, B., Schäbitz, F., 2014. Climate variability over the last 92 ka in SW Balkans from analysis of sediments from lake Prespa. Clim. Past 10, 643–660. https://doi.org/10.5194/cp-10-643-2014.
Poynter, J.G., Farrimond, P., Robinson, N., Eglinton, G., 1989. Aeolian-derived higher plant lipids in the marine sedimentary record: links with Palaeoclimate. In: Leinen, M., Sarnthein, M. (Eds.), Paleoclimatology and Paleometeorology:

Modern and Past Patterns of Global Atmospheric Transport, NATO ASI Series (Series C: Mathematical and Physical Sciences), vol. 282. Springer, Dordrecht. https://doi.org/10.1007/978-94-009-0995-3_18.
Rach, O., Brauer, A., Wilkes, H., Sachse, D., 2014. Delayed hydrological response to Greenland cooling at the onset of the Younger Dryas in western Europe. Nat. Geosci. 7, 109–112. https://doi.org/10.1038/ngeo2053.
Rao, Z., Zhu, Z., Wang, G., Jia, G., Qiang, M., Wu, Y., 2009. CPI values of terrestrial higher plant-derived long-chain n-alkanes: a potential paleoclimatic proxy. Front. Earth Sci. China 3 (3), 266–272. https://doi.org/10.1007/s11707-009-0037-1.
Rasmussen, S.O., Bigler, M., Blockley, S.P., Blunier, T., Buchardt, S.L., Clausen, H.B., Cvijanovic, I., Dahl-Jensen, D., Johnsen, S.J., Fischer, H., Gkinis, V., Guillevic, M., Hoek, W.Z., Lowe, J.J., Pedro, J.B., Popp, T., Seierstad, I.K., Steffensen, J.P., Svensson, A.M., Vallelonga, P., Vinther, B.M., Walker, M.J.C., Wheatley, J.J., Winstrup, M., 2014. A stratigraphic framework for abrupt climatic changes during the Last Glacial period based on three synchronized Greenland ice-core records: refining and extending the INTIMATE event stratigraphy. Quat. Sci. Rev. 106, 14–28. https://doi.org/10.1016/j.quascirev.2014.09.007.
Reimer, P.J., Austin, W.E., Bard, E., Bayliss, A., Blackwell, P.G., Ramsey, C.B., et al., 2020. The IntCal20 Northern Hemisphere radiocarbon age calibration curve (0–55 cal kBP). Radiocarbon 62 (4), 725–757. https://doi.org/10.1017/RDC.2020.41.
Rieley, G., Collier, R.J., Jones, D.M., Eglinton, G., 1991. The bio-geochemistry of Ellesmere Lake, UK—I: source correlation of leaf wax inputs to the sedimentary record. Org. Geochem. 17, 901–909. https://doi.org/10.1016/0146-6380(91)90031-E.
Rivas-Martínez, S., 1987. Mapa de las series de vegetación de España, escala 1: 400.000. Ministerio de Agricultura, Pesca y Alimentación, ICONA Madrid.
Rodríguez de Vera, C., Herrera-Herrera, A.V., Jambrina-Enríquez, M., Sossa-Ríos, S., González-Urquijo, J., Lazuen, T., Vanlandeghem, M., Alix, C., Monnier, G., Pajović, G., Tostevin, G., Mallol, C., 2020. Micro-contextual identification of archaeological lipid biomarkers using resin-impregnated sediment slabs. Sci. Rep. 10 (1), 1–14. https://doi.org/10.1038/s41598-020-77257-x.
Sachse, D., Radke, J., Gleixner, G., 2004. Hydrogen isotope ratios of recent lacustrine sedimentary n-alkanes record modern climate variability. Geochim. Cosmochim. Acta 68, 4877–4889. https://doi.org/10.1016/j.gca.2004.06.004.
Sachse, D., Radke, J., Gleixner, G., 2006. δ D values of individual n-alkanes from terrestrial plants along a climatic gradient – implications for the sedimentary biomarker record. Org. Geochem. 37, 469–483. https://doi.org/10.1016/j.orggeochem.2005.12.003.
Sachse, D., Billault, I., Bowen, G.J., Chikaraishi, Y., Dawson, T.E., Feakins, S.J., Freeman, K.H., Magill, C.R., McInerney, F.A., van der Meer, M.T.J., Polissar, P., Robins, R.J., Sachs, J.P., Schmidt, H.L., Sessions, A.L., White, J.W.C., West, J.B., Kahmen, A., 2012. Molecular paleohydrology: interpreting the hydrogen-isotopic composition of lipid biomarkers from photosynthesizing organisms. Annu. Rev. Earth Planet Sci. 40, 221–249. https://doi.org/10.1146/annurev-earth-042711-105535.
Schwark, L., Zink, K., Lechterbeck, J., 2002. Reconstruction of postglacial to early Holocene vegetation history in terrestrial Central Europe via cuticular lipid biomarkers and pollen records from lake sediments. Geology 30 (5), 463–466. https://doi.org/10.1130/0091-7613(2002)030<0463:ROPTEH>2.0.CO;2.
Shaw, D., 2017. Archaeobotanical results from Crvena Stijena. In: Whallon, Robert (Ed.), Crvena Stijena in Cultural and Ecological Context Multidisciplinary Archaeological Research in Montenegro, pp. 307–340.
Sinopoli, G., Masi, A., Regattieri, E., Wagner, B., Francke, A., Peyron, O., Sadori, L., 2018. Palynology of the last interglacial complex at Lake Ohrid: palaeoenvironmental and palaeoclimatic inferences. Quat. Sci. Rev. 180, 177–192. https://doi.org/10.1016/j.quascirev.2017.11.013.
Svensson, A., Andersen, K.K., Bigler, M., Clausen, H.B., Dahl-Jensen, D., Davies, S.M., Johnsen, S.J., Muscheler, R., Parrenin, F., Rasmussen, S.O., Röthlisberger, R., Seierstad, I., Steffensen, J.P., Vinther, B.M., 2008. A 60,000 year Greenland stratigraphic ice core chronology. Clim. Past 4, 47–57. https://doi.org/10.5194/cp-4-47-2008.
van Andel, T.H., Davies, W., 2003. Neanderthals and Modern Humans in the European Landscape during the Last Glaciation: Archaeological Results of the Stage 3 Project. McDonald Institute for Archaeological Research monographs, p. 265.
van Meerbeeck, C.J.V.C., Renssen, H., Roche, D.M.V.A.P., Wohlfarth, B., Bohncke, S.J.P., Bos, J.A.A., Engels, S., Helmens, K.F., Sáncez-Goñi, M.F., Svensson, A., Vandenberghe, J., 2011. The nature of MIS 3 stadial-interstadial transitions in Europe: new insights from model-data comparisons. Quat. Sci. Rev. 30 (25–26), 3618–3637. https://doi.org/10.1016/j.quascirev.2011.08.002.
Voelker, A.H.L., 2002. Global distribution of centennial-scale records for Marine Isotope Stage (MIS) 3: a database. Quat. Sci. Rev. 21 (10), 1185–1212. https://doi.org/10.1016/S0277-3791(01)00139-1.
Vogel, H., Wagner, B., Zanchetta, G., Sulpizio, R., Rosén, P., 2010. A paleoclimate record with tephrochronological age control for the last glacial-interglacial cycle from Lake Ohrid, Albania and Macedonia. J. Paleolimnol. 44, 295–310. https://doi.org/10.1007/s10933-009-9404-x.
Wang, M., Zhang, W., Hou, J., 2015. Is average chain length of plant lipids a potential proxy for vegetation, environment and climate changes? Biogeosci. Discuss. 12 (7), 5477–5501. https://doi.org/10.5194/bgd-12-5477-2015.
Wang, C., Eley, Y., Oakes, A., Hren, M., 2017. Hydrogen isotope and molecular alteration of n-alkanes during heating in open and closed systems. Org. Geochem. 112, 47–58. https://doi.org/10.1016/j.orggeochem.2017.07.006.
Weber, M., Scholz, D., Schröder-Ritzrau, A., Deininger, M., Spötl, C., Lugli, F., Mertz-Kraus, R., Peter Jochum, K., Fohlmeister, J., Stumpf, C.F., Riechelmann, D.F.C., 2018. Evidence of warm and humid interstadials in central Europe during early MIS 3 revealed by a multi-proxy speleothem record. Quat. Sci. Rev. 200, 276–286. https://doi.org/10.1016/j.quascirev.2018.09.045.
Whallon, R., 2017. Crvena Stijena in Cultural and Ecological Context Multidisciplinary Archaeological Research in Montenegro. National Museum of Montenegro Montenegrin Academy of Sciences and Arts, p. 463.
Whallon, R., Morin, E., 2017. Eleven years of research at Crvena Stijena: synthesis of the results. In: Whallon, Robert (Ed.), Crvena Stijena in Cultural and Ecological Context Multidisciplinary Archaeological Research in Montenegro, pp. 450–455.
Wiesenberg, G., Lehndorff, E., Schwark, L., 2009. Thermal degradation of rye and maize straw: lipid pattern changes as a function of temperature. Org. Geochem. 40, 167–174. https://doi.org/10.1016/j.orggeochem.2008.11.004.
Wirth, S.B., Sessions, A.L., 2016. Plant-wax D/H ratios in the southern European Alps record multiple aspects of climate variability. Quat. Sci. Rev. 148, 176. https://doi.org/10.1016/j.quascirev.2016.07.020.
Xie, S., Nott, C.J., Avsejs, L.A., Maddy, D., Chambers, F.M., Evershed, R.P., 2004. Molecular and isotopic stratigraphy in an ombotrophic mire for paleoclimate reconstruction. Geochim. Cosmochim. Acta 68, 2849–2862. https://doi.org/10.1016/j.gca.2003.08.025.
Živković, K., Lojen, S., Pucarević, M., 2020. Overview of the chemical and isotopic investigations of the Mareza springs and the Zeta river in Montenegro. Water 12 (4), 957. https://doi.org/10.3390/w12040957.